Production of protons, deuterons, tritons in argon-nucleus interactions at 3.2 AGeV

BM@N Collaboration

Abstract

Physics results of the BM@N experiment at the Nuclotron/NICA complex are presented on studies of proton , deuteron and triton production in interactions of an argon beam with fixed targets of C, Al, Cu, Sn and Pb at 3.2 AGeV. Transverse mass distributions, rapidity spectra and multiplicities of protons, deuterons, tritons are measured. The results are treated within a coalescence approach and compared with predictions of theoretical models and with other measurements.

1 Introduction

BM@N (Baryonic Matter at Nuclotron) is the first operational experiment at the Nuclotron/NICA accelerator complex. The Nuclotron will provide beams of a variety of particles, from proton up to gold ions, with kinetic energy in the range from 1 to 6 GeV/nucleon for light ions with Z/A ratio of ~ 0.5 and up to 4.5 GeV/nucleon for heavy ions with Z/A ratio of ~ 0.4. At these energies, the nucleon density in the fireball created in the collisions of a heavy-ion beam with fixed targets is 3-4 times higher than the nuclear saturation density [1], thus allowing studying heavy-ion interactions in the regime of high-density baryonic matter [2].

The primary goal of the experiment is to constrain the parameters of the equation of state (EoS) of high-density nuclear matter [3] and to search for the conjectured critical end point, the onset of the deconfinement phase transition and the onset of the chiral symmetry restoration [4, 5].

In the commissioning phase, in a configuration with limited phase-space coverage, BM@N collected first experimental data with beams of carbon, argon, and krypton ions [6,7]. In the first physics paper BM@N reported on studies of π^+ and K^+ production in argon-nucleus interactions [8] This paper presents first results on proton, deuteron and triton production in 3.2 AGeV argon-nucleus interactions.

The incoming nucleon loses its momentum during the collision and the mechanism of baryon transfer over finite rapidity distances (baryon stopping [12]) is an important theoretical problem for many years [13]- [15]. The baryon density, attained in high energy nuclear collisions, is a crucial quantity governing the reaction dynamics and the overall system evolution, including eventual phase transformations in dense nuclear matter. The measurement of rapidity distributions of stopped baryons in heavy ion collisions for different combinations of projectile and target as well as at different impact parameters provides essential constrains for the possible dynamical scenarios of baryon charge transfer. The advantage of the BM@N experiment at NICA is that the experimental arrangement of the detector makes it possible to measure the distribution of protons and light nuclei (d, t) over a rapidity interval [1.0 - 2.2]. This rapidity range is wide enough to include particle rapidity density not only near the midrapidity (y_{CM} = 1.08), but also at the rapidity of the incoming nucleus, in contrast to the situation at the collider, where the acceptance of collider experiments does not include this range. Together with a sufficient p_T-coverage for nuclear clusters in BM@N, it makes possible to better determine the shape of the rapidity density distribution and derive information about rapidity and energy loss in the reaction.

Nuclear cluster production allows one to estimate the nucleon phase-space density attained in the reaction. It governs the overall evolution of the reaction process and may provide information about freeze-out conditions and entropy production in relativistic nucleus-nucleus interactions. A way to measure the nucleon phase-space density is the study of the ratio of deuteron and proton abundances. One among the goals of this work is the study of particle phase-space density evolution in Ar+A collisions for different projectile-target combinations and as a function of collision centrality.

In the framework of statistical thermal models, hadron and light nuclei abundances are predicted to be dependent on the bulk parameters of the fireball: the freeze-out temperature T and baryochemical potential μ [9]. The ratio μ/T can be extracted from the characteristic parameter (penalty factor) describing the mass dependence of the yields of cluster. In this paper, we will study the system size and mass dependence of the cluster production to get insight about thermal parameters of the particle source.

In collisions of heavy nuclei at relativistic energies, a significant fraction of the initial kinetic energy transformed into particle production and thermal excitation of matter. Various dynamical models, including those based on hydrodynamic description, have demonstrated that the created during the initial interaction stage entropy per baryon S/A remains constant during the subsequent evolution of the system [25, 26]. Thus, data about entropy production can provide information not only about the nucleon phase-space density at the final moments of the reaction (freezeout), but also about the medium properties during the hot and compressed stage. It is also the aim of this work to study the evolution of the entropy in the reaction zone with system size in argon-nucleus collisions and compare BM@N results with exciting experimental data.

The binding energies of deuterons and tritons are small compared to freeze-out temperatures, which are on the order 100 MeV. These light clusters are therefore not expected to survive through the high density stages of the collision. The deuterons and tritons observed in the experiment are formed and emitted near freeze-out, and they mainly carry information about this late stage of the collision.

The heavy-ion experimental data on light cluster production at low energies are well described in a simple coalescence model [37–39] through the distributions of their constituents (protons and neutrons) and an coalescence parameter B_A related to the size A of the cluster. To describe heavy-ion collisions at high energies the simple coalescence model should be modified. In the modified approach, the production of nucleon clusters depends on the nucleon phase space distributions at freeze-out as well as on the strength of momentum-space correlations induced by collective flow [40]. In central heavy-ion collisions the pressure gradient in the system generates strong transverse radial flow. Therefore nucleon clusters inside a collective velocity field acquire additional momentum proportional to the cluster's mass. The strength of the radial flow measured in interactions of middle-size nuclei at the Nuclotron beam energy of few AGeV could be compared to the results obtained in heavy ion collisions at lower and higher energies.

The paper is organized as follows. Section 2 describes the experimental set-up and Section 3 is devoted to details of the event reconstruction. Section 4 describes the evaluation of the proton, deuteron, triton reconstruction efficiency. Section 5 explains the method for definition of the centrality classes. Section 6 addresses the evaluation of the cross sections, multiplicities and systematic uncertainties. Experimental results on transverse mass distributions and rapidity spectra of protons, deuterons, tritons are given in Section 7. The BM@N results are compared with predictions of theoretical models. Ratios of the transverse momentum distributions of deuterons and tritons to protons are treated within a coalescence approach in section 8. The results are compared with other experimental data on nucleus-nucleus interactions. The compound ratios of yields of protons and tritons to deuterons are presented in section 10. Finally, the results are summarized in Section 11.

2 Experimental set-up

The BM@N detector is a forward spectrometer covering the pseudorapidity range $1.6 \leq \eta \leq 4.4$. A schematic view of the BM@N setup in the argon-beam run is shown in Fig. 1. More details of all components of the set-up can be found in [41, 42]. The spectrometer includes a central tracking system consisting of 3 planes of forward silicon-strip detectors (ST) and 6 planes of detectors based on gas electron multipliers (GEM) [43]. The central tracking system is located downstream of the target region inside of a dipole magnet with a bending power of about $\approxeq 2.1$Tm and with a gap of 1.05 m between the poles . In the measurements reported here, the central tracker covered only the upper half of the magnet acceptance.

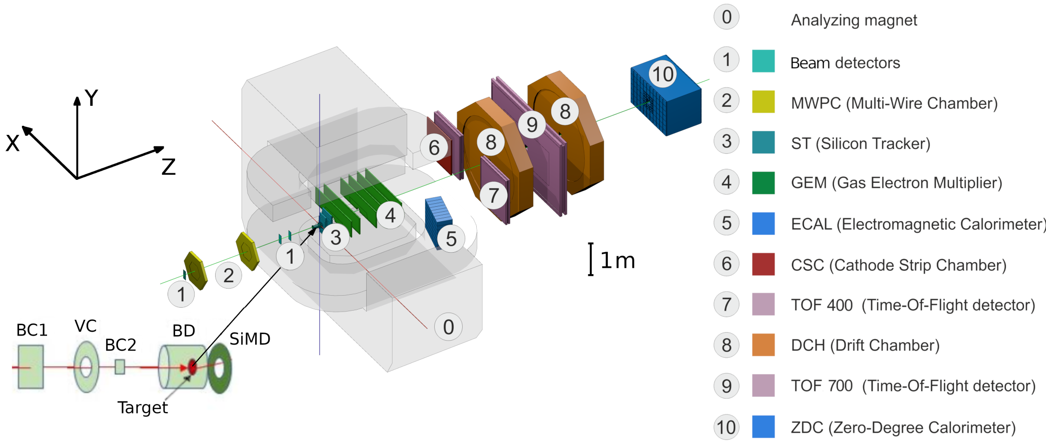

Figure 1: Schematic view of the BM@N setup in the argon beam run.

Two sets of drift chambers (DCH), a cathode strip chamber (CSC), two sets of time-of-flight detectors (ToF), and a zero-degree calorimeter (ZDC) are located downstream of the dipole magnet. The tracking system measures the momentum of charged particles with a relative uncertainty that varies from 2.5% at a momentum of 0.5 GeV/c to 2% from 1 to 2 GeV/c and rises linearly to 6.5% at 5 GeV/c. The time resolutions of the ToF-400 and ToF-700 systems are 84 ps and 115 ps, respectively [44].

Two beam counters (BC1, BC2), a veto counter (VC), a barrel detector (BD), and a silicon multiplicity detector (SiMD) were used for event triggering and for measurement of the incoming beam ions. The BC2 counter provided also the start time T0 for the time of flight measurement. The BD detector consists of 40 azimuthal scintillating strips arranged around the target, and the SiMD detector consists of 60 azimuthal silicon segments situated behind the target.

To count the number of beam ions that passed through the target, a logical beam trigger $\mathrm{BT} = \mathrm{BC1} \wedge \overline{\mathrm{VC}} \wedge \mathrm{BC2}$ was used. The following logic conditions were applied to generate the trigger signal: 1) BT$\wedge$(BD$\geq 3, 4$); 2) BT$\wedge$(SiMD$\geq 3, 4$); 3) BT$\wedge$(BD$\geq$ 2)$\wedge$(SiMD$\geq$ 3). The trigger conditions were varied to find the optimal ratio between the event rate and the trigger efficiency for each target. Trigger condition 1 was applied for 60% of the data collected with the carbon target. This trigger fraction was continuously reduced with the atomic weight of the target down to 26% for the Pb target. The fraction of data collected with trigger condition 2 was increased from 6% for the carbon target up to 34% for the Pb target. The rest of the data were collected with trigger condition 3. The analysis presented here used the data from the forward silicon detectors, GEM detectors, outer drift chambers, cathode strip chamber, and the two sets of the time-of-flight detectors ToF-400 [45] and ToF-700 [46]. Data were collected with an argon beam intensity of a few 10^5 ions per spill and a spill duration of 2–2.5 sec. The kinetic energy of the beam was 3.2 AGeV with the spread of about 1%. A set of solid targets of various materials (C, Al, Cu, Sn, Pb) with a relative interaction length of

3% was used. The experimental data correspond to an integrated luminosity of 7.8 μb^{-1} collected with the different targets: 2.1 μb^{-1} (C), 2.3 μb^{-1} (Al), 1.8 μb^{-1} (Cu), 1.1 μb^{-1} (Sn), 0.5 μb^{-1} (Pb). A total of 16.3M argon-nucleus collisions at 3.2 AGeV were reconstructed.

3 Event reconstruction

Track reconstruction in the central tracker is based on a "cellular automaton" approach [47] implementing a constrained combinatorial search of track candidates with their subsequent fitting by a Kalman filter to determine the track parameters. These tracks are used to reconstruct primary and secondary vertices as well as global tracks by extrapolation and matching to hits in the downstream detectors (CSC, DCH and ToF).

The primary collision vertex position (PV) is measured with a resolution of 2.4 mm in the X-Y plane perpendicular to the beam direction and 3 mm in the beam direction at the target position.

Charged particles (protons, deuterons, tritons) are identified using the time of flight Δt measured between T0 and the ToF detectors, the length of the trajectory Δl and the momentum p reconstructed in the central tracker. Then the squared mass M^2 of a particle is calculated by the formula: $M^2 = p^2((\Delta tc/\Delta l)^2 - 1)$, where c is the speed of light.

Candidates of protons, deuterons, tritons must originate from the primary vertex and match hits in the CSC and ToF-400 or in the DCH and ToF-700 detectors. The following criteria are required for selecting proton, deuteron, triton candidates:

- Each track has at least 4 hits in the GEM detectors (6 detectors in total) [43]. Hits in the forward silicon detectors are used to reconstruct the track, but no requirements are applied to the number of hits;

- Tracks originate from the primary vertex. The deviation of the reconstructed vertex from the target position along the beam direction is limited to -3.4 cm $< Z_{\rm ver} - Z_0 <$ 1.7 cm, where Z_0 is the target position. The upper limit corresponds to $\sim 5.7\sigma$ of the Z_{ver} spread and cuts off interactions with the trigger detector located 3 cm behind the target. The two vertical lines in the figure limit the region of the Z coordinates accepted for the data analysis for all the targets. The beam interaction rate with the trigger detector is well below 1% and was not simulated since it does not affect the precision in Monte Carlo simulation.

- Distance from a track to the primary vertex in the X-Y plane at Z_{ver}(DCA) is required to be less than 1 cm, which corresponds to 4σ of the vertex resolution in the X-Y plane;

- Momentum range of positively charged particles $p > 0.5$ GeV/c and $p > 0.7$ GeV/c is limited by the acceptance of the ToF-400 and ToF-700 detectors, respectively;

- Distance of extrapolated tracks to the CSC (DCH) hits as well as to the ToF-400 (ToF-700) hits should be within $\pm 2.5\sigma$ of the momentum dependent hit-track residual distributions.

The spectra of the mass squared (M^2) of positively charged particles produced in interactions of the 3.2 AGeV argon beam with various targets are shown in Figs. 2a and 2b for ToF-400 and ToF-700 data, respectively. The proton, deuteron, triton signals are extracted in the M^2 windows which depend on rapidity and at the maximal rapidity extend from 0.4-1.7 $(\mathrm{GeV/c^2})^2$, 2.3-5.0 $(\mathrm{GeV/c^2})^2$ and 6.6-10.0 $(\mathrm{GeV/c^2})^2$, respectively. The signals of protons, deuterons, tritons and their statistical errors are calculated according to the formulae: $sig = hist - bg$, $err_{stat} = \sqrt{hist + bg}$, assuming the background uncertainty is $\sqrt{bg}$. Here $hist$ and bg denote the histogram and background integral yields within the selected M^2 windows.

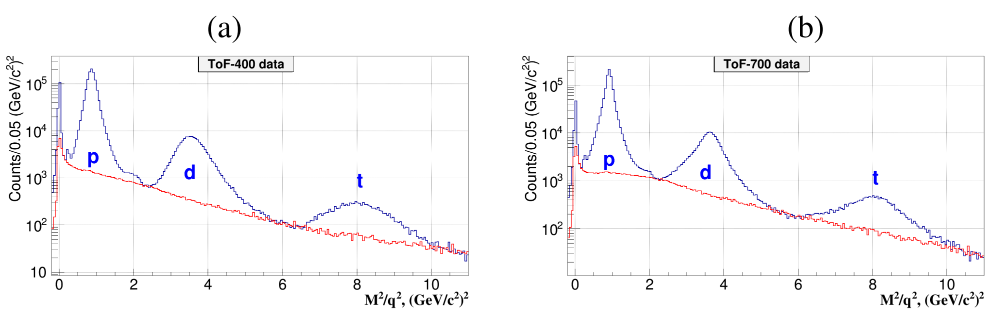

Figure 2: M^2 spectra of positively charged particles produced in argon-nucleus interactions and measured in the ToF-400 (a) and ToF-700 (b) detectors. Peaks of protons, deuterons, tritons are indicated. The red histograms show the background estimated from "mixed events".

The shape of the background under the proton, deuteron, triton signals in the M^2 spectra is estimated using the "mixed event" method. For that, tracks reconstructed in the central tracker are matched to hits in the ToF detectors taken from different events containing similar number of tracks. The "mixed event" background is normalized to the integral of the signal histogram outside the M^2 windows of protons, deuterons, tritons. It is found that the background level differs for light and heavy targets and for different intervals of rapidity and transverse momentum.

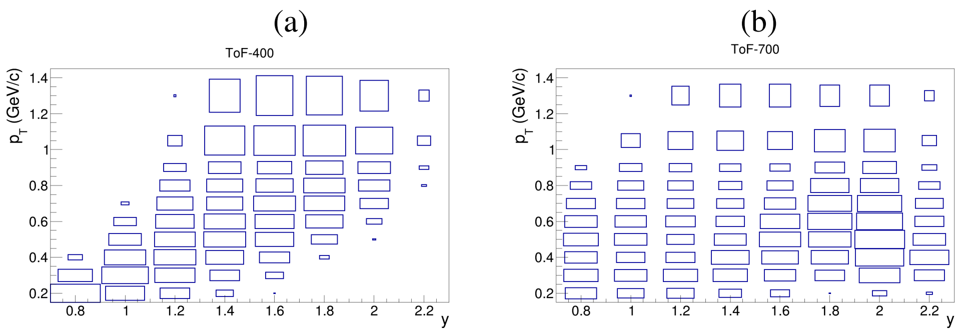

Figure 3: Distribution of the deuteron signals measured in ToF-400 (a) and ToF-700 (b) in the rapidity and transverse momentum bins in Ar+Sn interactions.

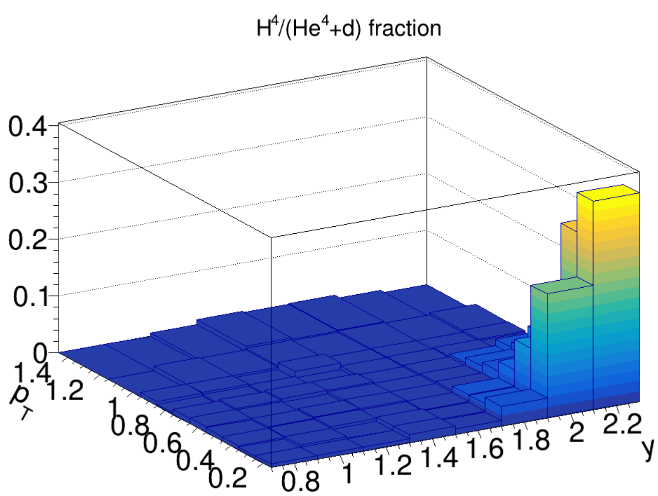

Figure 4: Fraction of He^4 in the $He^4 + d$ sample measured in the rapidity and transverse momentum bins in Ar+A interacions.

The ToF-400 and ToF-700 detectors cover different ranges of rapidity and transverse momentum of detected particles. Fig. 3 shows the signals of deuterons measured in ToF-400 and ToF-700 in the rapidity vs transverse momentum plane in Ar+Sn interactions before making corrections for the efficiency.

Using the dE/dx information from the GEM detectors the deuteron signals are separated from the He^4 signals. Fraction of He^4 in the total $He^4 + d$ sample is calculated in the rapidity and transverse momentum bins and subtracted from the data signals. The He^4 fraction combined for all the targets is presented in Fig. 4. In most of the $y - p_T$ bins the He^4 fraction does not exceed 3%, only in few bins at large y and low p_T it reaches 20-35%.

4 Reconstruction efficiency and trigger performance

To evaluate the proton, deuteron, triton reconstruction efficiency, Monte Carlo data samples of argon-nucleus collisions were produced with the DCM-SMM event generator [49, 50]. Propagation of particles through the entire detector volume and responses of the detectors were simulated using the GEANT3 program [51] integrated into the BmnRoot software framework [52]. To properly describe the GEM detector response in the magnetic field, the Garfield++ toolkit [53] for simulation of the micropattern gaseous detectors was used.

The efficiencies of the forward silicon, GEM, CSC, DCH and ToF detectors were adjusted during simulation in accordance with the measured detector efficiencies [54]. The Monte Carlo events went through the same chain of reconstruction and identification as the experimental events.

The level of agreement between the Monte Carlo and experimental distributions is demonstrated on a set of observables: closest distance from a track to the primary vertex in the X-Y plane (DCA), χ^2/NDF, number of reconstructed tracks at the primary vertex and number of hits per track (Figs. 5a–d).

The proton, deuteron, triton reconstruction efficiencies are calculated in intervals of rapidity y and transverse momentum p_T. The reconstruction efficiency includes the geometrical acceptance, the detector efficiency, the kinematic and spatial cuts, the loss of protons, deuterons, tritons due to in-flight interactions. The reconstruction efficiencies of protons and deuterons detected in ToF-400 and ToF-700 are shown in Fig. 6 as functions of y (upper panel) and p_T (lower panel) for Ar+Sn interactions.

The trigger efficiency ϵ_{trig} depends on the number of fired channels in the BD (SiMD) detectors. It was calculated for events with reconstructed protons, deuterons, tritons using event samples recorded with an independent trigger based on the SiMD (BD) detectors. The BD and SiMD detectors cover different and non-

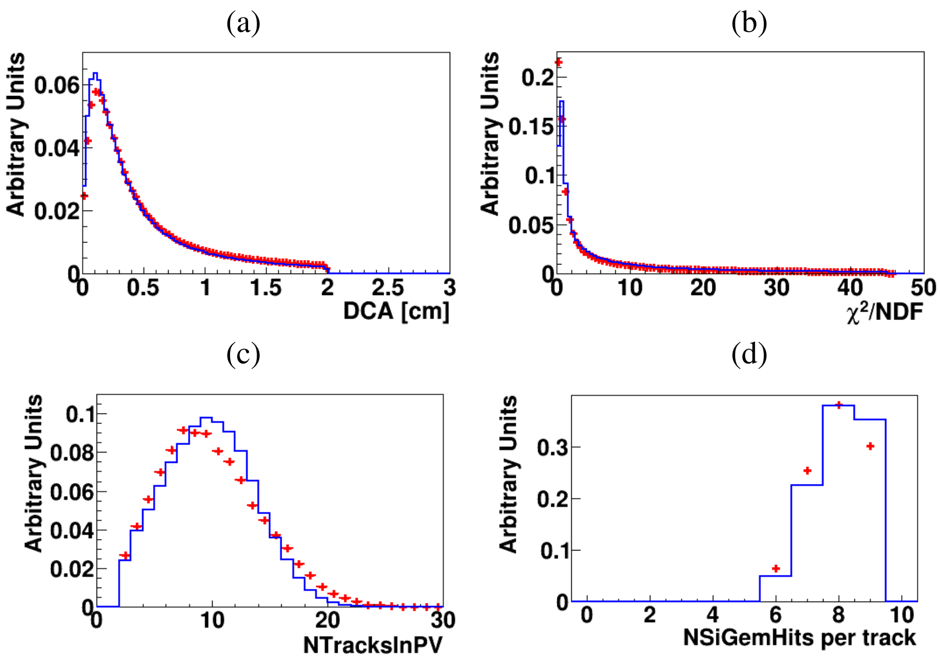

Figure 5: Comparison of experimental distributions (red crosses) and GEANT distributions of events generated with the DCM-SMM model (blue lines), in Ar+A collisions at 3.2 AGeV: (a) DCA, distance of closest approach to the primary vertex; (b) χ^2/NDF of reconstructed tracks; (c) number of reconstructed tracks in the primary vertex in Ar+Cu interactions; (d) Hits per track in the 3 forward Si and 6 GEM detectors.

overlapping regions of the BM@N acceptance, that is, they detect different collision products. For the BD trigger efficiency estimation, the following relation is used: ϵ_{trig} (BD $\geq$ m) = N(BD $\geq$ m $\wedge$ SiMD $\geq$ n)/N(SiMD $\geq$ n), where m and n are the minimum number of fired channels in BD (m = 3, 4) and SiMD (n = 3, 4) (see Section 2). A similar relation is used to evaluate the SiMD trigger efficiency. The BD (SiMD) trigger efficiency is averaged over all data with the different values of the minimum number of fired channels in SiMD (BD).

The efficiency of the combined BD and SiMD triggers was calculated as the product of the efficiencies of the BD and SiMD triggers. The trigger efficiency decreases with a decrease in the mass of the target and an increase in the centrality of the collision. More details of the trigger efficiences evaluation are given in paper [8].

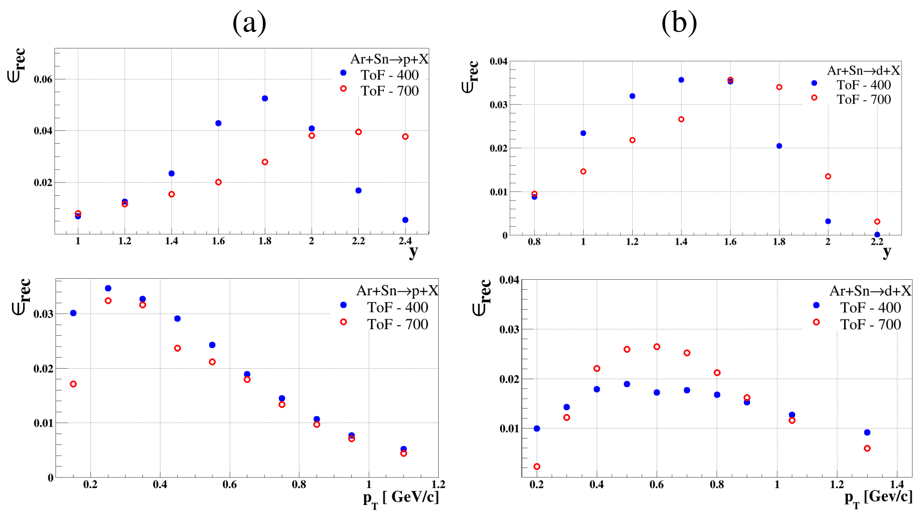

Figure 6: Reconstruction efficiency of protons (a) and deuterons (b) produced in Ar+Sn collisions, detected in ToF-400 (full blue circles) and ToF-700 (open red circles) as functions of rapidity y and p_T. The efficiency includes both acceptance and reconstruction.

5 Centrality classes

The event centrality is determined as the fraction of the interaction cross section in the interval $[0, \mathrm{b}]$ of the impact parameter b of the nucleus-nucleus collision to the total inelasic interaction cross section. Two classes of centrality: 1) 0-40% of the cross section (more central collisions) and 2) 40-100% of the cross section (more peripheral collisions), are defined from the impact parameter distributions of Ar+A inelasic interactions simulated by the DCM-SMM model. The boundary impact parameter b_{cut} for definition of two classes of centrality for interactions of Ar with various targets is given in Table 2. It was found that the number of tracks originated from the primary event vertex N(tracks) and the number of hits in the Barrel Detector N(BD) are anti-correlated with the impact parameter b of a nucleus-nucleus collision. Using results of the DCM-SMM Monte Carlo simulation, fractions of reconstructed events, which belong to the centrality classes 0-40% and 40-100%, are calculated. Fractions of events with centrality 0-40% and 40-100% are presented in Fig. 7 as functions of N(tracks) , N(BD) and as a two-dimensional distribution N(tracks) / N(BD).

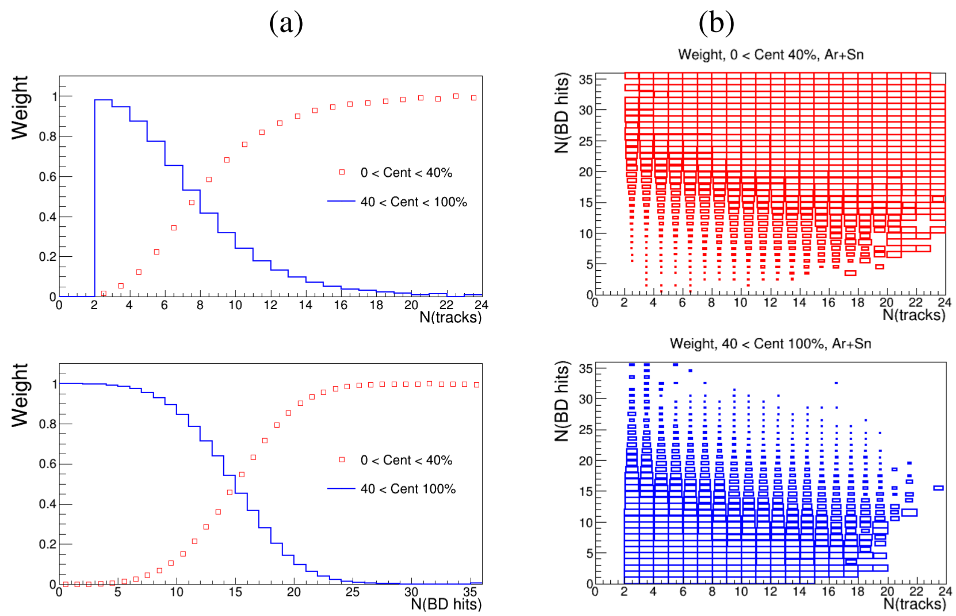

Figure 7: (a) Fraction (probability) of events with centrality 0-40% (red open symbols) and 40-100% (blue histogram) as a function of the number of tracks N(tracks) in the primary vertex (upper plot) and the number of hits N(BD) in the BD detector (lower plot). (b) two-dimensional distribution of the fraction (probability) of events with centrality 0-40% (upper red histogram) and 40-100% (lower blue histogram) as a function of N(tracks) (horizontal axis) and N(BD) (vertical axis).

Fractions (probabilities) of events with centrality 0-40% and 40-100%, taken from the two-dimensional N(tracks) / N(BD) distributions are used as event weights to define the weighted number of reconstructed protons, deuterons, tritons in the y and p_T bins in data and simulation. The systematic uncertainty of the event centrality is estimated from the remaining difference in the shape of the N(tracks) and N(BD) distributions in y and p_T bins in the simulation relative to the data.

6 Cross sections, multiplicities, and systematic uncertainties

The protons, deuterons and tritons in Ar+C, Al, Cu, Sn, Pb interactions are measured in the following kinematic ranges: transverse momentum $0.1 < p_T < 1.2$ GeV/c (protons), $0.15 < p_T < 1.45$ GeV/c (deuterons), $0.2 < p_T < 1.6$ GeV/c (tritons) and rapidity in the laboratory frame $0.9 < y < 2.5$ (protons), $0.7 < y < 2.3$ (deuterons), $0.7 < y < 2.1$ (tritons).

The analysis takes into account the track dependence of the trigger efficiency. No significant variation in the reconstruction efficiency with the track multiplicity was found. The differential cross sections $d^2\sigma_{p,d,t}(y, p_T)/dydp_T$ and multiplicities $d^2N_{p,d,t}(y, p_T)/dydp_T$ of protons, deuterons, tritons produced in Ar+C, Al, Cu, Sn, Pb interactions are calculated using the relations:

$$d^2\sigma_{p,d,t}(y, p_T)/dydp_T = \Sigma[d^2n_{p,d,t}(y, p_T, N_{tr})/(\epsilon_{trig}(N_{tr})dydp_T)] \times 1/(L\epsilon^{rec}_{p,d,t}(y, p_T))$$

$$d^2N_{p,d,t}(y, p_T)/dydp_T = d^2\sigma_{p,d,t}(y, p_T)/(\sigma_{inel}dydp_T) \quad (1)$$

where the sum is performed over bins of the number of tracks in the primary vertex, N_{tr}, $n_{p,d,t}(y, p_T, N_{tr})$ is the number of reconstructed protons, deuterons, tritons in the intervals dy and dp_T, $\epsilon_{trig}(N_{tr})$ is the track-dependent trigger efficiency, $\epsilon^{rec}_{p,d,t}$ is the reconstruction efficiency of protons, deuterons, tritons, L is the luminosity and σ_{inel} is the inelastic cross section for argon-nucleus interactions. The cross sections and multiplicities are evaluated for two classes of a collision centrality: 0-40% and 40-100%.

Table 1 summarizes the mean values, averaged over p_T, y and N_{tr} of the systematic uncertainties of the various factors of Eq. (1), $n_{p,d,t}$, ϵ_{rec}, and ϵ_{trig}. Details are given below, including the uncertainty of the luminosity measurement. The model uncertainty of σ_{inel} is given in Table 2.

Several sources are considered for the evaluation of the systematic uncertainty of the proton, deuteron, triton yield, $n_{p,d,t}$, and the reconstruction efficiency ϵ_{rec}. The most significant ones are discussed below. Some of them affect both the yield $n_{p,d,t}$ and the reconstruction efficiency, ϵ_{rec}. For these cases the correlated effect is taken into account by the variations on the $n_{p,d,t}/\epsilon_{rec}$ ratio:

- Systematic uncertainty of the central tracking detector efficiency: it is estimated from the remaining difference in the number of track hits in the central detectors in the simulation relative to the data (see Fig. 5d) and found to be within 3%.
- Systematic uncertainty of the matching of central tracks to the CSC (DCH) hits and ToF-400 (ToF-700) hits: it is estimated from the remaining difference in the matching efficiency in the simulation relative to the data and found to be within 5%.
- Systematic uncertainty of the reconstruction efficiency due to the remaining difference in the X/Y distribution of primary vertices in the simulation relative to the data.

- Systematic uncertainty of the background subtraction in the mass-squared M^2 spectra of identified particles: it is estimated as the difference between the background integral under the p, d, t mass-squared windows taken from "mixed events" (as described in Section 3) and from the fitting of the M^2 spectra by a linear function. The latter is done in the M^2 range, excluding the proton, deuteron, triton signal windows.
- Systematic uncertainty calculated as half of the difference of the proton, deuteron, triton yields measured in bins of rapidity y in the ToF-400 and ToF-700 detectors
- Systematic uncertainy of the event centrality weights estimated 1) from the remaining difference in the shape of the N(track) and N(BD) distributions in the y and p_T bins in the data and the simulation; 2) from the difference in the event centrality weights taken from the two-dimensional N(track) / N(BD) distribution relative to the one-dimensional N(BD) distribution.

The total systematic uncertainty of the yield and reconstruction efficiency for the various targets, calculated as the quadratic sum of these uncertainties, is listed in Table 1.

The luminosity is calculated from the beam flux Φ as given by the beam trigger (see Section 2) and the target thickness l using the relation: $L = \Phi\rho l$ where ρ is the target density expressed in atoms/cm^3. The systematic uncertainty of the luminosity is estimated from the fraction of the beam which can miss the target, determined from the vertex positions, and found to be within 2%.

For the evaluation of the systematic uncertainty of the trigger efficiency ϵ_{trig}, the following sources are considered:

- The systematic uncertainty associated with the factorization assumption of the two trigger factors, BD and SiMD, was estimated from the difference of ϵ_{trig} evaluated as described in Section 4, with the result evaluated using the limited amount of events registered with the beam trigger BT.
- To estimate a possible distortion of ϵ_{trig} (BD $\geq$ m) due to the selection of events with the hardware-set condition N(SiMD $\geq$ n), ϵ_{trig} was also evaluated using the events recorded with the beam trigger BT. The difference between the results is treated as another source of systematic uncertainty of the trigger efficiency.
- Variations of the trigger efficiency on the track multiplicity in the primary vertex and on the X/Y vertex position.

The total systematic uncertainty of the trigger efficiency for the various targets, calculated as the quadratic sum of these uncertainties, is listed in Table 1.

The inelastic cross sections of Ar+C, Al, Cu, Sn, Pb interactions are taken from the predictions of the DCM-SMM model which are consistent with the results calculated by the formula: $\sigma_{inel} = \pi R_0^2 (A_P^{1/3} + A_T^{1/3})^2$, where $R_0 = 1.2$ fm is the effective nucleon radius, A_P and A_T are the atomic numbers of the projectile and target nucleus [55]. The systematic uncertainties for the Ar+C, Al, Cu, Sn, Pb inelastic cross sections are estimated from an alternative formula [56] which approximates the measured nucleus-nucleus cross sections: $\sigma_{inel} = \pi R_0^2 (A_P^{1/3} + A_T^{1/3} - b)^2$ with $R_0 = 1.46$ fm and $b = 1.21$ The values and uncertainties of σ_{inel} for Ar+C, Al, Cu, Sn, Pb interactions are given in Table 2.

7 Rapidity and mean transverse mass spectra

At a kinetic energy of 3.2 GeV/nucleon, the rapidity of the nucleon-nucleon center-of-mass (CM) system is $y_{CM} = 1.08$. The rapidity intervals covered in the present measurements, $0.9 < y < 2.5$, $0.7 < y < 2.3$ and $0.7 < y < 2.1$ for protons, deuterons, tritons, respectively, correspond therefore to the forward and central rapidity regions in the nucleon-nucleon CM system. The yields of protons, deuterons, tritons measured in the m_T and y bins in two centrality intervals of Ar+C,Al,Cu,Sn,Pb interactions are summarized at [48].

Table 1: Mean systematic uncertainties in y, p_T bins of protons, deuterons, tritons measured in argon-nucleus interactions (see text for details).

	Ar+C %	Ar+Al %	Ar+Cu %	Ar+Sn %	Ar+Pb %
ϵ_{trig} p,d,t	9	7	7	7	7
protons					
n_p, ϵ_{rec}	15	6	8	14	11
Total	18	9	11	16	13
deuterons					
n_d, ϵ_{rec}	32	22	20	19	22
Total	33	23	21	20	23
tritons					
n_t, ϵ_{rec}	43	22	20	20	22
Total	44	23	21	21	23

The transverse mass $m_T = \sqrt{m_{p,d,t}^2 + p_T^2}$ spectra of protons, deuterons, tritons produced at rapidity $y = 1.4$ in collisions with centrality 0-40% at various targets are shown in Figs. 15. The spectra are parameterised by an exponential function as:

$$1/m_T \cdot d^2N/dydm_T = \frac{dN/dy}{T_0(T_0+m)} \cdot \exp(-(m_T - m)/T_0) \quad (2)$$

where fitting parameters are the integral of the m_T spectrum, dN/dy, and the inverse slope, T_0. The rapidity spectra of protons, deuterons, tritons produced in collisions with centrality 0-40% at various targets are shown in Figs. 16a, 17a and 18a, respectively. The dN/dy values integrated over entire p_T are extracted from the fit. It is seen that the spectra are softer in interactions with heavier targets. The experimental results are compared with predictions of the DCM-SMM [49, 50] and PHQMD [58] models. For protons, the models have quite similar predictions, which are in reasonable agreement with the experimental results in the forward rapidity range. At mid-rapidity the models under-estimate the data for interactions with the targets heavier than the carbon.

The spectra of deuterons and tritons dominate in the beam fragmentation range for Ar+C and Ar+Al interactions, whereas the spectra become more central for interactions with heavier targets. For deuterons and tritons, the models reasonably describe the shape of the experimental spectra, but under-predict the normalization of the data by factors of 4 and 6, respectively. The rapidity spectra of protons, deuterons, tritons produced in collisions with centrality 40-100% at various targets are shown in Figs. 16b, 17b and 18b, respectively. The largest contribution is observed in the beam fragmentation range for all the targets. This tendency is reproduced by the DCM-SMM and PHQMD models, but the models under-

Table 2: The boundary impact parameter b_{cut} for definition of two classes of centrality, 0-40% and 40-100%, in inelastic Ar+A interactions. The inclusive cross section σ_{inel} for inelastic Ar+A interactions.

	Ar+C	Ar+Al	Ar+Cu	Ar+Sn	Ar+Pb
b_{cut}, fm	4.23	4.86	5.66	6.32	7.10
σ_{inel}, mb [55]	1470 ± 50	1860 ± 50	2480 ± 50	3140 ± 50	3940 ± 50

estimate the normalization of the data for deuterons and tritons by factors 4 and 5, respectively. The STAR experiment compared the yields of protons and light nuclei in fixed target Au+Au interactions at 0-10% centrality with predictions of the PHQMD model and presented a significant deficit of deuterons and tritons in the model relative to the experimental data [59].

The observed discrepancy between data and model predictions can in part be explained by the feeddown from the excited nuclear states. At BM@N collision energies, the reaction zone consists of a hadronic gas which is dominated by nucleons and stable compound systems ($d, t,^{3}$He, ^{4}He). However, in addition to stable nuclei there are many excited nuclear states which start from the mass number A=4. The role of the feeddown from these states for the description of light nuclei production in a broad energy range was discussed in Ref. [10]. A quantitative estimate of the feeddown contributions to deuterons and tritons was performed in the framework of a hadron resonance gas model, supplemented by a list of A=4 and A=5 excited nuclear states from [11]. As reported in [10], feeding gives significant contribution to the yields of d, t at NICA/BM@N energies: as much as 60% of all final tritons and 20% of deuterons may come from the decays of excited nuclear states. Since the feeding is not taken into account in the results of models, it might be a part of the reason for the underestimation of particle yields.

The mean transverse kinetic energy, expressed as $\langle E_T \rangle = \langle m_T \rangle - m$, is related to the T_0 value extracted from the fit of the m_T spectrum by the following equation:

$$\langle E_T \rangle = \langle m_T \rangle - m = T_0 + T_0^2/(T_0 + m).$$

The $\langle E_T \rangle$ values obtained from the fits of the proton spectra in the y bins are shown in Fig. 19a for centrality 0-40%. The maximal values of $\langle E_T \rangle$ are measured at rapidity $1.0 < y < 1.3$, i.e. at mid-rapidity in the CM system. In general, the y dependence of $\langle E_T \rangle$ for protons is consistent with predictions of the DCM-SMM and PHQMD models.

The $\langle E_T \rangle$ values for deuterons and tritons obtained in the y bins for centrality 0-40% are shown in Figs. 19b and 19c, respectively. The PHQMD model reproduces the rise of the data at mid-rapidity in CM for deuterons and tritons relative to protons, where as the DCM-SMM model predicts similar $\langle E_T \rangle$ values for protons, deuterons and tritons in contradiction with the experimental results.

Figure 20 shows the BM@N results for the mid-rapidity value of the mean transverse kinetic energy, $\langle E_T \rangle$, for protons, deuterons and tritons produced in argon-nucleus collisions with centrality 0-40%. The mid-rapidity value of $\langle E_T \rangle$ is calculated as the average value for three points at y=1.0, 1.2 and 1.4. Assuming the $m_T/\cosh y^*$ dependence of the transverse mass on the CM rapidity y^*, the maximal $\langle E_T \rangle$ value is only 2% higher of the measured averaged value. It is seen, that $\langle E_T \rangle$ rises approximately linearly with the mass of the nuclear fagment. For the Ar+C colliding system no mass dependence of the $\langle E_T \rangle$ value is observed.

The mean transverse kinetic energy could be expressed as a sum of the energy of radial flow and random thermal motion as [63]:

$$\langle E_T \rangle \approx E_{therm} + E_{flow} = 3/2T^* + (\gamma - 1)m \quad (3)$$

where $\gamma = 1/\sqrt{1 - \langle \beta \rangle^2}$, $\langle \beta \rangle$ is the average radial collective velocity and T^* is the temperature of the thermal motion. In order to separate the contributions from random thermal and radial collective motion the data on $\langle E_T \rangle$ at each target are parameterized with two fit parameters: T^* and $\langle \beta \rangle$. However, the extrapolation of linear fits to zero mass (i.e. the parameter T^*) cannot be directly related to the source temperature since the temperature in expanding fireballs is blue shifted as:

$$T^* = T\sqrt{(1 + \langle \beta \rangle)/(1 - \langle \beta \rangle)} \quad (4)$$

Thus, in order to obtain the true temperature, the T^* parameter is corrected by the blue-shift factor according to equation 4. The average radial velocity $\langle \beta \rangle$ and source temperature at the kinetic freeze-out extracted from these fits are given in Table 3. In Ar+C interactions BM@N observes no collective radial flow, i.e. $\langle \beta \rangle \sim 0$. The BM@N results for T and $\langle \beta \rangle$ measured for interactions of middle-size nuclei (from Ar+Al to Ar+Pb) are lower compared with $T \sim 95 - 110$ MeV and $\langle \beta \rangle \sim 0.46$ measured in the NA-49 [63] and STAR BES [64] experiments in interactions of heavy nuclei (Pb+Pb and Au+Au) at higher energies. The FOPI experiment measured $T \sim 100$ MeV and $\langle \beta \rangle \sim 0.35$ in Au+Au collisions at 1.2 AGeV and found that the radial flow decreases rapidly in interactions of middle-size nuclei [65]. The BM@N results are consistent with the general tendency of the thermal temperature and radial flow to rise with the collision system size and energy.

8 Coalescence factors

Within a coalescence model [37, 38] nuclear fragment formation is characterized by a coalescence factor B_A, defined through the invariant momentum spectra by the equation:

$$E_A d^3N_A/d^3p_A = B_A(E_p d^3N_p/d^3p)^Z (E_n d^3N_n/d^3p)^{A-Z}_{|p=p_A/A} \quad (5)$$

where p_A and $p = p_A/A$ are momenta of the nuclear fragment and the nucleon, respectively. It relates the yield N_A of nuclear fragments with charge Z and atomic mass number A to the yields of the coalescing nucleons N_p and N_n at the same velocity. It has been assumed that the neutron momentum density is equivalent to the proton momentum density at freeze-out. The B_A value is then calculated in the variables y and p_T:

$$B_A = d^2N_A/2\pi p_{T,A}dp_{T,A}dy/(d^2N_p/2\pi p_T dp_T dy)^A \qquad (6)$$

In a thermodynamic approach [60, 61] B_A is inversely related to the fireball volume in coordinate space: $B_A \sim V_{eff}^{1-A}$. In accordance with model expectations [40] strong position-momentum correlations present in the expanding source lead to a higher coalescence probability at larger values of p_T. Assuming a box-like transverse density profile of the source, the model predicts:

$$B_A \propto \exp[m_T(1/T_p - 1/T_A)]/(m_T R_{\parallel}(m_T)R_{\perp}^2(m_T))^{A-1} \qquad (7)$$

where $R_{\perp}$ and $R_{\parallel}$ are the HBT radii of the source [40], T_p and T_A are the transverse momentum slopes for proton and nucleus A. Figs. 21a and 21b show the B_2 and B_3 values as a function of the transverse momentum measured in argon-nucleus interactions with centrality 0-40%. The transverse momentum is normalized to the atomic number of the nuclear fragment (deuteron, triton), p_T/A. The yields of protons (N_p), deuterons (N_d) and tritons (N_t) are measured in the same rapidity range, namely $0.9 < y < 1.7 (-0.18 < y^* < 0.62)$. Statistics of tritons are not sufficient to present B_3 for Ar+C interactions. It is found, that B_2 and B_3 are rising with p_T for all the measured targets, but the dependence is close to linear rather than exponential. The B_2 and B_3 values at low p_T are smaller for heavier targets compared to lighter targets.

Table 3: T and $\langle\beta\rangle$ values evaluated from the linear fit of the $\langle E_T\rangle = \langle m_T\rangle - m$ values of protons, deuterons and tritons produced in Ar+A interactions with centrality 0-40%.

	Ar+C	Ar+Al	Ar+Cu	Ar+Sn	Ar+Pb
T , MeV	89 ± 3	76 ± 8	80 ± 5	74 ± 9	80 ± 10
$\langle\beta\rangle$	0.0 ± 0.04	0.26 ± 0.05	0.27 ± 0.03	0.30 ± 0.04	0.26 ± 0.05

In order to compare the present measurements of B_2 and B_3 with previously obtained results, the $B_2(p_T)$ and $B_3(p_T)$ values given in Figs. 21a and 21b are extrapolated down to $p_T = 0$ using an exponential fit of the form $B_A(p_T = 0)\exp(a \cdot p_T)$ as it is predicted by the coalescence model (see equation 7). To evaluate the uncertainty of the parameter $B_A(p_T = 0)$ the data errors are scaled by a factor $\sqrt{\chi^2/ndf}$ from the first iteration of the fit. The results of the extrapolation are given in Table 4. The BM@N values of B_2 and B_3 are compared in Fig.22a,b with the measurements of other experiments. The B_2 and B_3 results for Ar+A interactions with centrality 0-40% are consistent with the energy dependence of the B_2 and B_3 factors for central interactions of heavy nuclei, as compiled in [63], [68], [72], [74]. It can be seen, that the BM@N measurements follow a general trend of decreasing B_2 and B_3 values with rising energy of heavy ion collisions. The B_2 and B_3 values are inversely related to the coalescence radius R_{coal} which is closely related to the HBT radii of the source of produced deuterons and tritons [40]. Using prescriptions in [62] based on [40], the coalescence source radius $R_{coal} = \sqrt[3]{3/2R_{\|}R_{\perp}^2}$ is calculated from the $B_2(p_T = 0)$ and $B_3(p_T = 0)$ values of deuterons and tritons. In calculations, the C_d and C_t factors from [62] are scaled according to the mass of colliding systems. The resulting values are in the range of 0.55-0.61 and 0.48-0.53 for deuterons and tritons, respectively. The results for R_{coal} are given in Table 4. The coalescence source radii for deuterons

Table 4: Coalescence parameters $B_2(p_T = 0)$ and $B_3(p_T = 0)$ extrapolated to $p_T = 0$ using an exponential fit to $B_2(p_T)$ and $B_3(p_T)$ for deuterons and tritons produced in Ar+A interactions with centrality 0-40%. Coalescence radii $R^d_{coal}(p_T = 0)$ and $R^t_{coal}(p_T = 0)$ evaluated from the $B_2(p_T = 0)$ and $B_3(p_T = 0)$ values for deuterons and tritons produced in Ar+A interactions with centrality 0-40%.

	Ar+C	Ar+Al	Ar+Cu	Ar+Sn	Ar+Pb
$B_2(p_T = 0)/10^3$, GeV^2/c^3	5.5 ± 1.9	1.7 ± 0.5	1.8 ± 0.4	1.2 ± 0.4	1.1 ± 0.2
$B_3(p_T = 0)/10^6$, GeV^3/c^4		1.7 ± 1.7	4.0 ± 1.2	2.7 ± 0.6	1.8 ± 0.4
$R_d(p_T = 0)$, fm	2.1 ± 0.3	3.1 ± 0.3	3.0 ± 0.2	3.5 ± 0.4	3.6 ± 0.2
$R_t(p_T = 0)$, fm		3.1 ± 0.5	2.7 ± 0.2	2.9 ± 0.1	3.1 ± 0.1

and tritons produced in Ar+Al,Cu,Sn,Pb interactions with centrality 0-40% are consistent with values of 3-3.5 fm except for deuterons produced in Ar+C interactions. The BM@N values for the coalescence radii averaged for Ar+Al,Cu,Sn,Pb interactions are compared in Fig.23 with results at higher energies as compiled in [63]. It is found that the BM@N results are in agreement with the energy dependence of the coalescence source radii of deuterons and tritons produces in heavy ion collisions. In general, the results are in qualitative agreement with the naive expectation of decreasing homogeneity lengths and a smaller effective volume in collisions of smaller systems and at lower energies.

9 Baryon rapidity distributions, stopping and rapidity loss in Ar+A

The total baryon number in Ar+A collisions at NICA/BM@N energies is basically determined by nucleons and light nuclei ($d, t,{}^3$He). To obtain the baryon rapidity distribution, we add up the yield of protons, deuterons and tritons in every rapidity bin. The measured yield for every particle sort was multiplied by the number of nucleons in the compound system. The number of nucleons bound in clusters contribute to the total number of baryons up to about 15% and 25% in central Ar+C and Ar+Pb reactions, respectively. The obtained distribution should then be corrected for the fraction of unmeasured baryons: neutrons, hyperons and ^{3}He nuclei. Calculations with the PHQMD and UrQMD models indicate that for all reactions the n/p-ratio is of about 1.1 in the forward hemisphere varying slowly with rapidity and then increasing abruptly to ≈1.22 (the n/p-ratio in the projectile Ar-nucleus) at the beam rapidity. We used these model predictions to estimate the yield of neutrons n, furthermore, we assume that the $t/{}^3$He ratio is equal to n/p. The total number of baryons B in a rapidity bin was then calculated as

$$B = p + n + 2.0 \cdot d + 5.7 \cdot t,$$

where the coefficient in front of t is 5.7 = 3.0 (for tritons) + 3.0/1.1 (for ^{3}He).

Hyperons contribute less than 2% to the baryons and were not accounted for. Resulting baryon rapidity distributions for Ar+Cu collisions are shown in Fig. 8 as a function of center-of-mass rapidity: the left panel shows the results for 0-40% central collisions, and the right one is for peripheral collisions. As one can see, more baryons are transported to midrapidity in the more central collisions leading to a dramatic difference in the shapes of dn/dy distributions. To describe those shapes, we fitted the measurements to a 3^{rd} order polynomial in y^2, and the fit results are shown in Fig. 8 by solid curves.

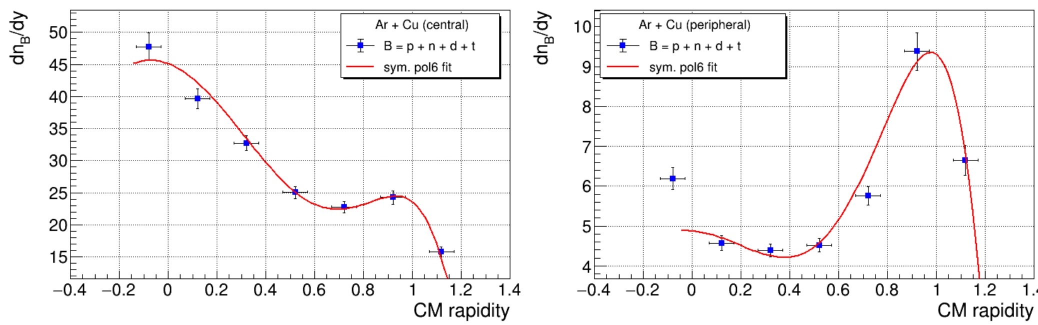

Figure 8: Left: Rapidity distribution of baryons in 0-40% central Ar+Cu collisions. The measurements are shown by symbols, a fit to a 3^{rd} order polynomial in y^2 is drawn by the curve. Right: same for peripheral Ar+Cu collisions.

The average rapidity loss is calculated as

$$\langle \delta y \rangle = y_b - \langle y \rangle, \tag{8}$$

where y_b is the rapidity of the projectile before the collisions, and

$$\langle y \rangle = \int_{y_0}^{y_b} y \frac{dn}{dy} dy \Bigg/ \int_{y_0}^{y_b} \frac{dn}{dy} dy \tag{9}$$

This equation refers to net-baryons, i.e. baryons minus antibaryons. At NICA energies, however, the production of antibaryons is so small that the difference between baryons and net-baryons is negligible. The low integration limit in Eq. 8 is the midrapidity ($y_0 = 0$), but, the calculation result is correct only for little mixing of projectile and target participants. Dealing with asymmetric Ar+A collisions from BM@N, however, we followed the suggestion from Ref. [18] and defined y_0 such that the area enclosed by the baryon dn/dy across the bounding values is equal to the number of participating nucleons in the projectile N_p^{proj}. These numbers of participants were determined from microscopic models. The y_0 value varies from 0.12 for Ar+Pb to -0.3 for Ar+C collisions.

The final $\langle \delta y \rangle$ values for central and peripheral collisions are listed in Table 5. The trend for the average rapidity loss is evident: $\langle \delta y \rangle$ is higher for heavier targets and increases with centrality.

Table 5: The average rapidity loss $\langle \delta y \rangle$ in Ar+A reactions

	Ar+C	Ar+Al	Ar+Cu	Ar+Sn	Ar+Pb
0-40%	0.47 ± 0.03	0.54 ± 0.03	0.60 ± 0.03	0.62 ± 0.04	0.64 ± 0.04
>40%	0.39 ± 0.03	0.42 ± 0.03	0.47 ± 0.03	0.53 ± 0.04	0.55 ± 0.04

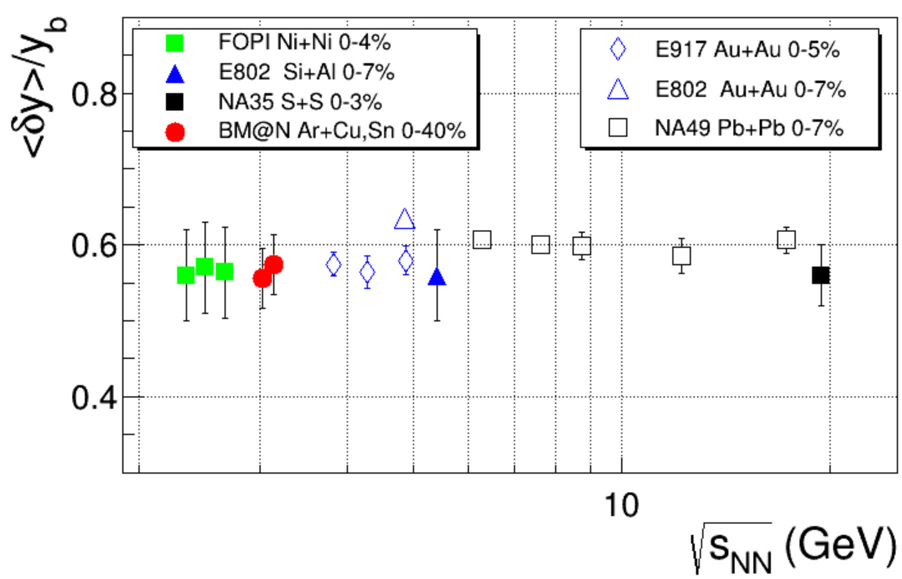

Figure 9: The excitation function of the scales average rapidity loss $\langle \delta y \rangle / y_b$ in ion-ion collisions. Medium-size colliding systems are drawn by solid symbols, while heavy systems are shown by open ones. Centrality intervals are indicated in the legends. BM@N points for Ar+Cu and Ar+Sn reactions are displaced horizontally for the clarity.

The energy dependence of nuclear stopping power is presented in Fig. 9, where the scaled average rapidity shift $\langle \delta y \rangle / y_b$ in ion-ion collisions is shown as a function of $\sqrt{s_{NN}}$. A collection of medium-size colliding systems from [16]- [19] is drawn by solid symbols and the corresponding centrality intervals are indicated in the legends. According to (purely geometrical) Glauber calculations, all presented medium-size reactions (despite of the different collision centrality) have approximately the same number of collisions per participating nucleon $N_{col/N_{part}} \approx 1.2-1.5$. Thus, for the comparison with world data, we selected only Ar+Cu $((N_{col}/N_{part} = 1.3)$ and Ar+Sn $((N_{col}/N_{part} = 1.4)$ reactions. The chosen BM@N points are slightly displaced along the x-axis for the clarity of presentation. As one can see, the shape of the baryon rapidity spectra from medium size collision systems does not vary over a broad energy range. Surprisingly, the observations from heavy colliding systems [18, 19] also support the trend (see open symbols in Fig. 9). This contradicts our observation of a 65% gain in the average rapidity loss value from the peripheral Ar+C to the central Ar+Pb system (see Table 5). A possible (rather qualitative) explanation of this puzzling behavior might be that the increase in the number of nucleon-nucleon collisions in larger systems can be counterbalanced by nuclear transparency, which becomes prevalent at high collision energies.

10 Particle ratios

The rapidity and system size dependence of the deuteron-to-proton ratio R_{dp} in Ar+A collisions at $\sqrt{s_{NN}}$=3.1 GeV is presented in Fig. 10, a)-e). As one can see, R_{dp} rises strongly from the midrapidity to the beam rapidity in peripheral collisions. The same trend is observed in central Ar+C collisions. In contrast, in central collisions of argon nuclei with targets heavier than (or equal to) aluminium, R_{dp} indicates a plato-like behavior near the midrapidity. This saturation rapidity region for R_{dp} increases gradually with the target mass number covering almost the total forward rapidity region in central Ar+Pb collisions.

A collection of the midrapidity R_{dp} values from central and peripheral Ar+A collisions as a function of the midrapidity baryon density dn_B/dy is presented in Fig. 10, f). As one can see, R_{dp} in Ar+A increases steady with system size for small baryon multiplicities and then levels off at high dn_B/dy. For a system in chemical equilibrium and if the size of the emitting source is larger than the width of the deuteron wave function, the ratio of deuterons to protons can be related to the average proton phase-space density at the freezeout $\langle f_p \rangle$ as

$$\langle f_p \rangle = \frac{R_{pn}}{3} \frac{E_d \frac{d^3 N_d}{d^3 P}}{E_p \frac{d^3 N_p}{d^3 p}} \qquad (10)$$

where R_{pn} is proton-to-neutron ratio, $P = 2p$, and the factor of 3 accounts for the spins of the particles [20]. The $\langle f_p \rangle$ value depends on the strength of nuclear stopping in the reaction as well as on the outward flow effects in a hot, dense medium. Thus, the observed in Fig. 10, f) trend can be understood qualitatively as follows. On the one hand, the proton phase-space density reached in the reaction zone is the lower the more peripheral the collision process is, taking both the size of the deuteron cluster and the participant volume into account. On the other hand, the baryon stopping (making fireball more dense) and radial expansion (causing the baryons occupy a bigger volume and spread over a wider momentum range) can balance each other in central collisions of argon nuclei with heavy target at NICA energies causing a saturation of $\langle f_p \rangle$.

Furthermore, Fig. 11 shows the evolution of the average proton's phase-space density as a function of transverse momentum. Here, the particle yield ratios are obtained in the rapidity range 0.05$< y <$0.45 and at three p_T/A values: 0.15, 0.3, and 0.45 GeV/c; the $\langle f_p \rangle$ value was calculated according to Eq. 10. The values of the R_{pn} ratio in the chosen phase-space region were taken from the UrQMD model. Some data points in the figure are displaced along the x-axis for the clarity. In a thermal source at a low phase-space density ($f << 1$) $\langle f_p \rangle$ follows a Bolzmann distribution and decreases exponentially with p_T [22]. If, however, outward flow is present in the system, $f(p_T)$ may become flatter [23]. Taking into account results on the radial velocity and temperature presented in Table 3 (i.e. little radial expansion in Ar+C and approximately same values of T and β in Ar+Al,Cu,Sn,Pb are indicated), one can conclude that the observed in Fig 11 trend is indeed consistent with the expectations.

It was identified long time ago that the nuclear cluster abundances and the entropy value attained in the collisions are related. According to early investigations [27], for the mixture of nucleons and deuterons in thermal and chemical equilibrium the entropy per nucleon S_N/A can be deduced from the deuteron-to-proton ratio R_{dp} as

$$\frac{S_N}{A} = 3.945 - \ln R_{dp} - \frac{1.25 R_{dp}}{1 + R_{dp}} \qquad (11)$$

Furthermore, as the collision energy increases, the contribution of mesons to the total entropy S_π becomes important. Following [30], the entropy of pions per

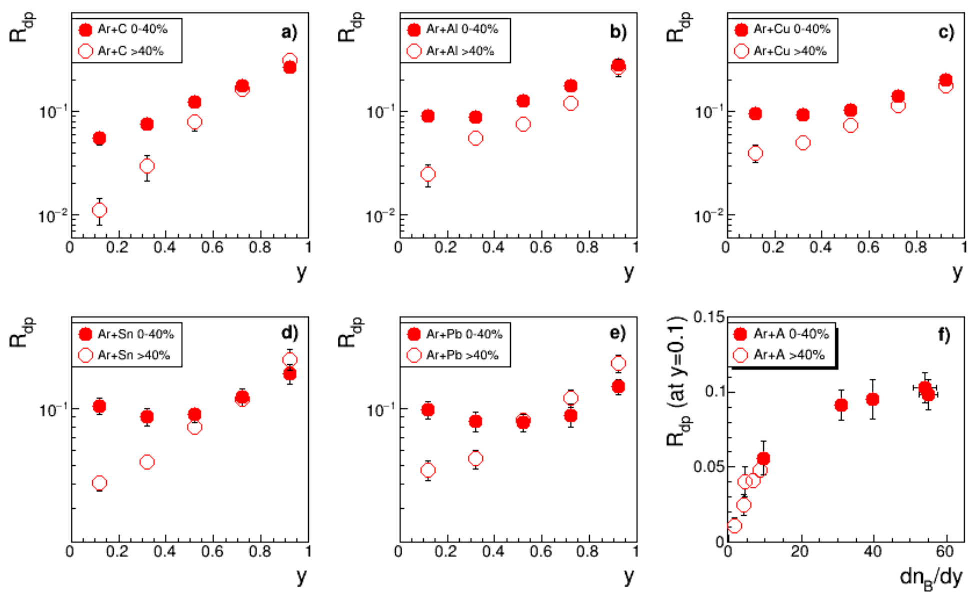

Figure 10: R_{dp} as a function of center-of-mass rapidity y in Ar+C (a), Ar+Al (b), Ar+Cu (c), Ar+Sn (d), and Ar+Pb (e) collisions. Central and peripheral collisions are shown by solid and open symbols, respectively. f): Midrapidity R_{dp} as a function of midrapidity baryon density dn_B/dy in Ar+A collisions.

.

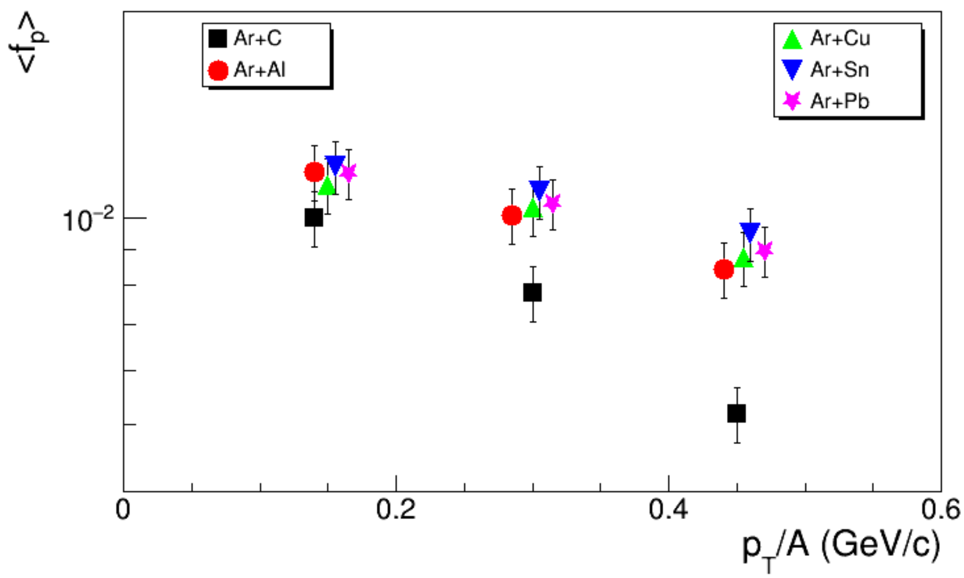

Figure 11: Average proton phase-space density for central Ar+A collisions as a function of p_T/A within the rapidity range 0.05$<y<$0.45. The shown results are obtained at $p_T = 0.15, 0.3, 0.45$ GeV/c, but displaced horizontally for the clarity.

nucleon can be estimated by

$$\frac{S_\pi}{A} = 4.1\frac{N_\pi}{N_N}, \tag{12}$$

where $N_N = N_p + N_n$ is the total number of nucleons.

As a result, we calculated the total entropy S/A as a sum of the nucleon and pion entropy contributions according to Eq. 11 and Eq. 12. Also, it should be noted that we used data on the particle yields near midrapidity. To estimate S_π, we used recently published BM@N results on positively charged pions [8], while the contribution of π^-, π^0, and neutrons was obtained from the UrQMD model. We found that the contribution of pions to the total entropy does not exceed 25% in the Ar+A reactions at NICA energies. Finally, S/A is found to be 10.6, 8.0, 8.0, 7.9, and 8.0 in central Ar+C, Ar+Al, Ar+Cu, Ar+Sn, and Ar+Pb, respectively. The estimated uncertainty for S/A is about 15%. In Fig. 12 we present the energy dependence for S/A in central heavy-ion collisions. This compilation includes data from those experiments which have published numerical values for the midrapidity yields of charged pions, protons, and light nuclei [16], [31], [32], [33], [34], [63], [66]. In this plot, We drawn the BM@N 'saturation' S/A-value of 8.0. As can be seen from the figure, the total entropy increases steady with collisions energy.

It has been established experimentally that cluster production yields decrease exponentially with the atomic mass number A [28, 63]. As an example, Fig. 13 (left panel) presents mid rapidity dn/dy for $p, d.t$ as a function of A from 0-40% central Ar+Sn collisions. The A-dependence of the yields was fitted to a form:

$$\frac{dn}{dy}(A) = const/p^{A-1}, \tag{13}$$

where parameter p ('penalty factor') determines the penalty of adding one extra nucleon to a system.

The penalty factor is sensitive to the nucleon density attained in the reaction (the larger density the smaller penalty) and in the framework of a statistical approach it is determined as follows

$$p = e^{(m-\mu_B)/T}, \tag{14}$$

where μ_B, T, and m being the baryochemical potential, freezeout temperature, and nucleon mass, respectively.

The p-factors from central Ar+A collisions are listed in Table 6 and shown in Fig. 13 (right panel) as a function of the midrapidity baryon density. The trend for

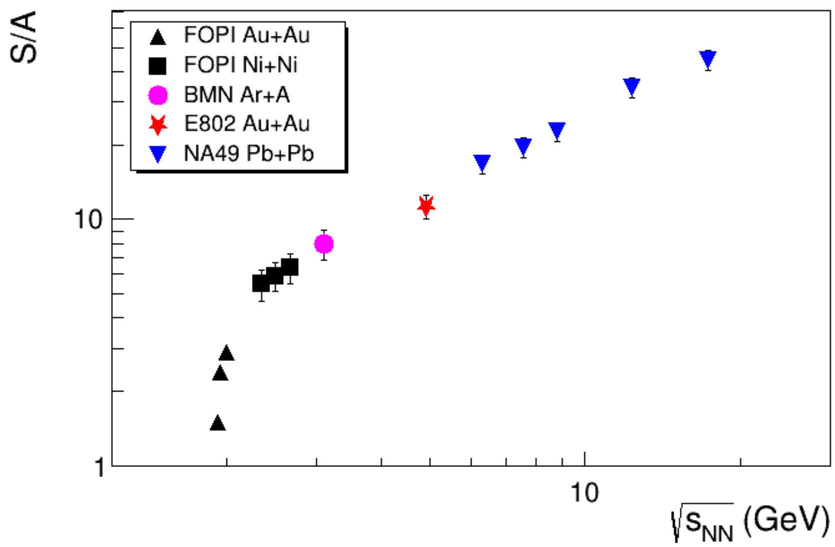

Figure 12: The excitation function of the entropy per baryon S/A from SIS/FOPI [16], [31], AGS/E802 [32], SPS/NA49 [33], [34], [63], [66] and NICA/BM@N (this study).

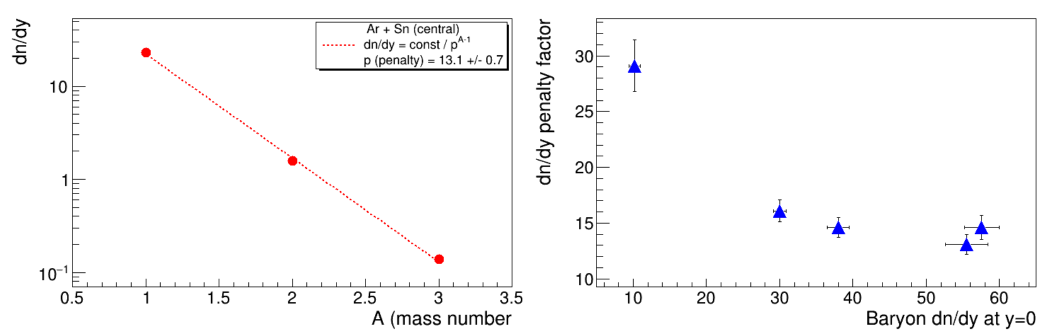

Figure 13: Left: Midrapidity dn/dy for p, d, t from central Ar+Sn collisions. The dashed line is a fit to Eq. 13. Right: Penalty factor from central Ar+A collisions versus baryon rapidity density at $y = 0$.

Table 6: Penalty factor p, temperature T (from Table 3), and baryochemical potential μ_B in 0-40% central Ar+A collisions.

	p	T (MeV)	μ_B(MeV)
Ar+C	29.1 ± 2.3	89 ± 3	638 ± 12
Ar+Al	16.1 ± 1.0	76 ± 8	727 ± 23
Ar+Cu	14.6 ± 0.7	80 ± 5	724 ± 14
Ar+Sn	13.1 ± 0.7	74 ± 9	748 ± 24
Ar+Pb	14.6 ± 0.8	80 ± 10	724 ± 27

the penalty is evident from the figure: p is decreasing for small baryon densities attained in Ar+C and Ar+Al reactions and then saturates above dn/d$y \approx 30$.

A standard method for the determination of the source thermodynamic freeze-out parameters T and μ_B is based on the analysis of hadron abundances in the framework of a thermal statistical model (see [36] and references therein). An alternative approach is the use of Eq. 14. As reported in Ref. [35], the values of kinetic and chemical freeze-out temperatures are similar in heavy-ion collisions below $\sqrt{s_{NN}} = 5$ GeV. Thus, we can use the value of T obtained in the analysis of transverse mass spectra of particles and listed in Table 3 as an estimate for a 'universal' freeze-out temperature. Re-arranging Eq. 14, one can write a formula for μ_B as

$$\mu_B = m - T \ln p \tag{15}$$

The resulting (T, μ_B) freeze-out parameters for central Ar+A collisions are tabulated in Table 6 and shown in Fig. 14. Surprisingly, the BM@N results follow the trend defined by world data and describing by the parameterization from Ref. [36] (which is drawn by the dashed line) with the only exception of Ar+C system being probably too small to obtain a globally equilibrated fireball.

Recently, measurements are performed by the STAR experiment to study the compound yield ratio $R_{ptd} = N_p \cdot N_t/N_d^2$ of protons (N_p) and tritons (N_t) to deuterons (N_d) [68]. Based on coalescence models, it is predicted [70] that the non-monotonic behaviour of the ratio as a function of the size of the system or collision energy is a signature of the neutron density fluctuations Δn: $R_{ptd} \approx g(1 + \Delta n)$ with a color factor $g \simeq 0.29$. Following this argument, R_{ptd} is a promising observable to search for the signature of the Critical Point and/or a first-order phase transition in heavy-ion collisions [69]. In coalescence models, the compound yield ratio should increase as the size of the system decreases. Indeed, this effect is observed by the STAR experiment [72].

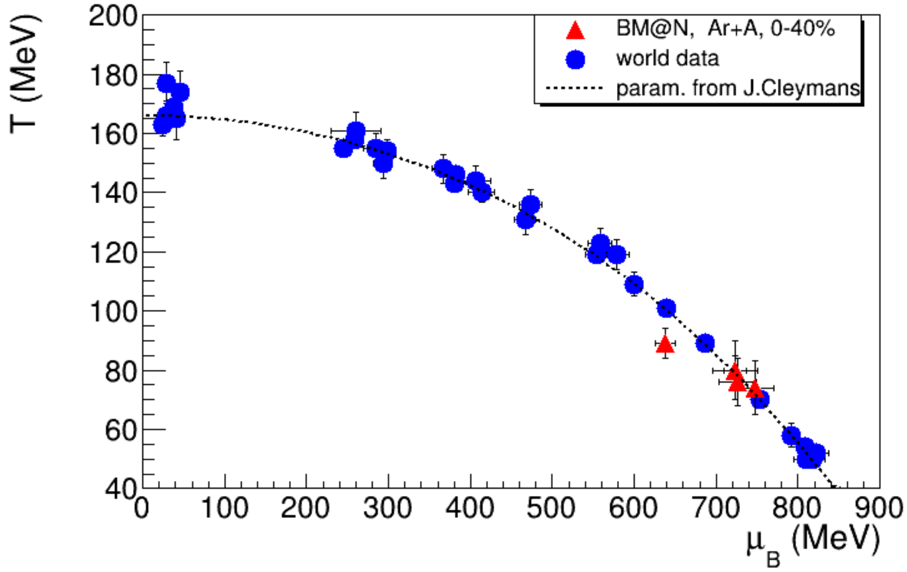

Figure 14: Freeze-out (T, μ_B) parameters for A+A collisions. BM@N results are from this study, world data and the parameterization for the freezeout line (dashed line) are from [36].

.

Table 7: $N_p \cdot N_t/N_d^2$ values evaluated from the dN/dy data of protons, deuterons and tritons produced in the rapidity range $-0.18 < y^* < 0.62$ in Ar+A interactions with centrality 0-40%.

	Ar+C	Ar+Al	Ar+Cu	Ar+Sn	Ar+Pb
$N_p \cdot N_t/N_d^2$	0.53 ± 0.10	0.55 ± 0.09	0.69 ± 0.11	0.60 ± 0.07	0.59 ± 0.06

To evaluate the R_{ptd} ratio, mean values of the dN/dy distributions for protons, deuterons and tritons are calculated in the rapidity range $0.9 < y < 1.7$ ($-0.18 < y^* < 0.62$). The results are given in Table 7 for argon-nucleus interactions with centrality 0-40%. Assuming the difference of the $N_p \cdot N_t/N_d^2$ values obtained for various targets from C to Pb as a systematic uncertainty, the weighted average value of the compound ratio is estimated to be 0.59 ± 0.09, where the uncertainty is the quadratic sum of the statistical and systematic uncertainties. Within the uncertainties there is no dependence of the R_{ptd} ratio on rapidity in the measured rapidity range. The BM@N value for R_{ptd} is compared in In Fig. 24 with the measurements of other experiments. The BM@N result lays between values of 0.8-1.0 derived from the FOPI data at lower energies and values of 0.4-0.5 obtained from the STAR and NA49 measurements at higher CM energies $\sqrt{s}$ from 6 to 18 GeV [74], [69], [71], [63].

11 Summary

First physics results of the BM@N experiment are presented on the proton, deuteron and triton yields and their ratios in argon-nucleus interactions at the beam kinetic energy of 3.2 AGeV. The results are compared with the DCM-SMM and PHQMD models and with the previously published results of other experiments.

The spectra of the transverse mass m_T are measured and the mean values $\langle m_T \rangle - m$ are presented for more central 0-40% events as functions of the rapidity y and mass of the nuclear fragment. The $\langle m_T \rangle - m$ values are found to depend linearly on the mass m. The results are parameterized as a function of the temperature and transverse velocity of the radial expansion of the source.

The rapidity spectra dN/dy of protons, deuterons and tritons are presented for the whole p_T range in two ranges of centrality. The DCM-SMM and PHQMD models reproduce shapes of the spectra, but underestimate the deuteron and triton yields by factors four and six, respectively.

We have analysed rapidity distributions of protons and light nuclei in central and peripheral Ar+A collisions. The average rapidity loss $\langle \delta y \rangle$ is larger for more heavy targets and increases with collision centrality. In contrast, the scaled to the beam rapidity $\langle \delta y \rangle$ value in medium-size heavy-ion collisions does not vary over a broad energy range indicating a non-trivial interplay of nucleon multiple scattering effects and nuclear transparency.

The ratio of deuterons to protons R_{dp} has been studied as a function rapidity in central and peripheral Ar+A collisions. The midrapidity R_{dp} rises in peripheral collisions and levels off in central ones. It may indicate a saturation of the nucleon phase-space density at the freezeout. In addition, the entropy per baryon S/A was estimated from the R_{dp} value and BM@N data on the charged pion production. $S/A \approx 8$ in central Ar+A collisions at NICA/BM@N energies and supports an increasing with collision energy trend.

The atomic mass dependence of cluster yields in central Ar+A collisions was investigated and the freezeout fireball parameters T and μ_B were obtained. We found that our results follow the trend defined by world data and by the thermal model parameterization for nucleus-nucleus collisions.

The deuteron to proton and triton to proton yield ratios are interpreted within a coalescence approach. The coalescence parameters B_2 and B_3 for deuterons and tritons are calculated in dependence on the transverse momentum p_T. The coalescence radii of the deuteron and triton source are extracted from the B_2 and B_3 values extrapolated to $p_T = 0$ and compared with results of other experiments. The compound yield ratio $N_p \cdot N_t/N_d^2$ of protons and tritons to deuterons is evaluated from the dN/dy spectra in the rapidity range $-0.18 < y^* < 0.62$. The result is compared with the values measured in heavy nucleus-nucleus collisions at lower and higher energies. The BM@N measurements follow a general trend of the decreasing B_2 and B_3 values and $N_p \cdot N_t/N_d^2$ ratio with the rising energy of heavy ion collisions.

Acknowledgments. The BM@N Collaboration acknowledges the efforts of the staff of the accelerator division of the Laboratory of High Energy Physics at JINR that made this experiment possible. The BM@N Collaboration acknowledges support of the HybriLIT of JINR for the provided computational resources.

References

[1] B. Friman, W. Nörenberg, and V.D. Toneev, Eur. Phys. J. A 3 (1998).

[2] J. Randrup and J. Cleymans, Phys. Rev. C 74 (2006) 047901.

[3] Ch. Fuchs, Prog. Part. Nucl. Phys. 56 (2006) 1-103.

[4] NICA White Paper, Eur. Phys. J. A 52 (2016).

[5] BM@N Conceptual Design Report: http://nica.jinr.ru/files/BM@N/BMN_CDR.pdf

[6] M. Kapishin (for the BM@N Collaboration), Nucl. Phys. A 982 (2019) 967-970.

[7] M. Kapishin (for the BM@N Collaboration), SQM 2019 proceedings, 285 Springer Proc. Phys. 250 (2020) 21-27.

[8] S. Afanasiev et al. (BM@N Collaboration), JHEP 07 (2023) 174.

[9] A. Andronic, P. Braun-Munzinger, and J. Stachel, Phys. Lett. B 673, 142 (2009).

[10] V.Vovchenko et al, Phys. Lett. B 809 (2020) 135746.

[11] D.R. Tilley, H.R. Weller, G.M. Hale, Nucl. Phys. A 541 (1992) 1.

[12] W. Busza and A. S. Goldhaber, Phys. Lett. 139B, 235 (1984).

[13] G.C. Rossi and G. Veneziano, Phys. Rep. 63 (1980) 153.

[14] A. Capella and B. Z. Kopeliovich, Phys. Lett. B 381, 325 (1996)

[15] D. Kharzeev, Phys. Lett. B 378, 238 (1996)

[16] B.Hong et al (FOPI Collaboration), Phys. Rev. C 57 (1998) 244.

[17] B.B.Back et al (E917 Collaboration), Phys. Rev. Lett. 86 (2001) 1970.

[18] F.Videbaek and Ole Hansen, Phys. Rev. C 52 (1995) 2684.

[19] C. Blume, for the NA49 Collaboration, J. Phys. G 34 (2007) S951.

[20] M.Murray and B. Holzer, Phys Rev. C 63, 054901 (2000).

[21] M. J. Bennett *et al* (E878 Collaboration) Rhys. Rev. C 58, 1155 (1998).

[22] M. J. Murray, J. Phys. G 28, 2069 (2002).

[23] B. Tomasik and U. Heinz, Phys. Rev. C 65, 031902(R) (2002).

[24] H. Schulz, G. Ropke, K. K. Gudima and V. D. Toneev, Phys. Rev. C 34, 1294 (1986).

[25] G. Bertsch and J. Cugnon, Phys. Rev. C 24, 2514 (1981).

[26] J. I. Kapusta, Phys. Rev. C 24, 2545 (1981).

[27] L. P. Csernai and J. I. Kapusta, Phys. Rep. 131, 4 (1986) 223—318.

[28] T.A. Armstrong et al (E864 Collaboration) Phys. Rev. C 61,064908 (2000).

[29] G. Bertsch and J. Cugnon, Phys. Rev. C 24, 2514 (1981).

[30] S. Z. Belenkij and L. D. Landau, Nuovo Cimento, Supplement 3, 15 (1956).

[31] G. Poggi et al (FOPI Collaboration), Nucl. Phys. A 586, 755 (1995).

[32] L. Ahle et al (E802 Collaboration) Phys. Rev. C 60, 064901 (1999).

[33] T. Anticic et al (NA49 Collaboration), Phys. Rev. C 69, 024902 (2004).

[34] C. Alt et al (NA49 Collaboration), Phys. Rev. C 77, 024903 (2008).

[35] The STAR Collaboration, Phys. Rev. C 96,044904 (2017).

[36] J. Cleymans, H. Oeschler, K. Redlich, and S. Wheaton, Phys. Rev. C 73, 034905 (2006).

[37] S.T. Butler and C.A. Pearson, Phys. Rev. 129, 836 (1963).

[38] A. Schwarzschild and C. Zupancic, Phys. Rev. 129, 854 (1963).

[39] S. Mrowczynski, Phys. Lett. B 277, 43 (1992).

[40] R. Scheibl and U. Heinz, Phys. Rev. C 59, 1585 (1999).

[41] BM@N project:
https://bmn.jinr.ru/detector/project/BMN_project.pdf

[42] S. Afanasiev et al., arXiv:2312.17573 [hep-ex]

[43] D. Baranov et al., JINST 12 (2017) no. 06, C06041

[44] K. Alishina et al., Phys. Part. Nucl., 53 (2022) no. 2, 470-475.

[45] V. Babkin et al., Nucl. Instrum. Meth. A 824, P.490-492 (2016); V. Babkin et al., Proceedings of Science, 2014, Vol.213 (Proceedings of TIPP-2014), P.289.

[46] N. Kuzmin et al., Nucl. Instrum. Meth. A 916, P. 190-194 (2019).

[47] V. Akishina and I. Kisel, J. Phys.: Conf. Ser. 599, 012024 (2015), I. Kisel, Nucl. Instrum. Meth. A 566, 85 (2006).

[48] BM@N web-page

[49] N. Amelin, K. Gudima, and V. Toneev, Sov. J. Nucl. Phys. 51, 1093 (1990).

[50] M. Baznat, A. Botvina, G. Musulmanbekov, V. Toneev, V. Zhezher, Phys. Part. Nucl. Lett. 17 (2020) no. 3; arXiv: 1912.09277v.

[51] CERN Program Library, Long Writeup W5013, Geneva, CERN, 1993.

[52] https://git.jinr.ru/nica/bmnroot

[53] http://garfieldpp.web.cern.ch/garfieldpp

[54] V. Plotnikov, L. Kovachev, A. Zinchenko, Phys. Part. Nuclei Lett. 20 (2023), 1392–1402

[55] K. Kanaki, PhD Thesis, Technische Universität Dresden, 2007.

[56] H. Angelov et al., P1-80-473, JINR, Dubna.

[57] S. A. Bass et al., Prog. Part. Nucl. Phys. 41 225 (1998).

[58] W. Cassing and E. L. Bratkovskaya, Nucl. Phys. A 831 (2009) 215-242.

[59] STAR Collaboration: [nucl-ex] arXiv:2311.11020

[60] A.Z. Mekjian, Phys. Rev. Lett. 38, 640 (1977); Phys. Rev. C 17, 1051 (1978); and Nucl. Phys. A 312, 491 (1978).

[61] J. I. Kapusta, Phys. Rev. C 21, 1301 (1980).

[62] I.G. Bearden et al., Eur. Phys. J. C 23, 237–247 (2002).

[63] T. Anticic et al. (NA49 Collaboration) Phys. Rev. C 94, 044906 (2016)

[64] L. Kumar (for the STAR Collaboration), Nucl. Phys. A 931, 1114 (2014)

[65] W.Reisdorf et al. (FOPI Collaboration) Nucl.Phys.A 848 (2010) 366-427

[66] T. Anticic et al. (NA49 Collaboration) Phys.Rev.C 85 (2012) 044913

[67] J. Adam et al. (STAR Collaboration) Phys. Rev. C 99, 064905

[68] M.Abdulhamid et al., STAR Collaboration, Phys.Rev.Lett. 130 (2023) 202301

[69] D.Oliinychenko, Nucl.Phys.A 1005 (2021) 121754

[70] K.-J.Sun et al., Phys.Lett.B 774 (2017) 103

[71] H.Liu et al., Phys.Lett.B 805 (2020) 135452, Phys.Lett.B 829 (2022) 137132 (erratum)

[72] D. Zhang (STAR Collaboration), Nucl. Phys. A 1005, 121825 (2021).

[73] M. Abdulhamid et al. (STAR Collaboration), Phys.Rev.Lett. 130 (2023) 202301.

[74] arXiv:2311.11020 [nucl-ex]

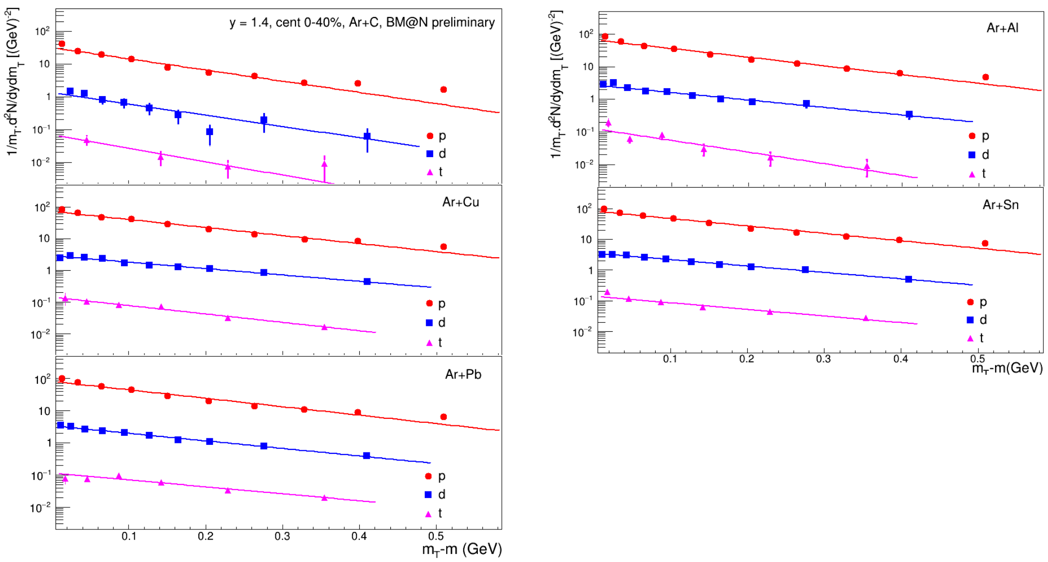

Figure 15: Transverse mass spectra of protons, deuterons, tritons produced at rapidity $y = 1.4$ in Ar+C, Al, Cu, Sn, Pb interactions with centrality 0-40%. The vertical bars and boxes represent the statistical and systematic uncertainties, respectively. The lines show the results of the fit by an exponential function.

(a)

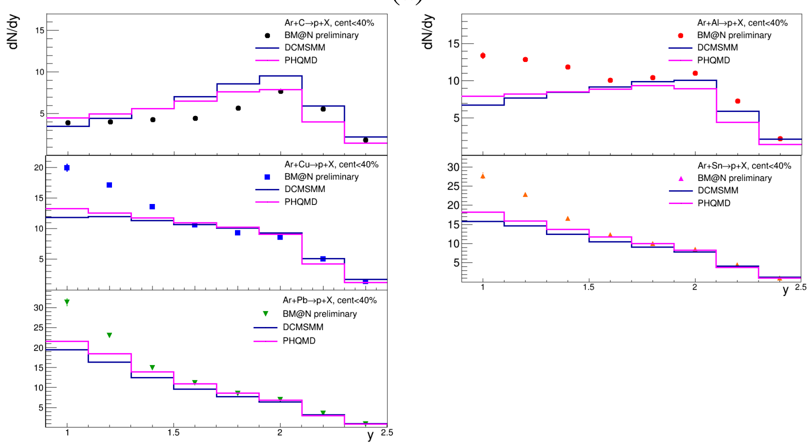

(b)

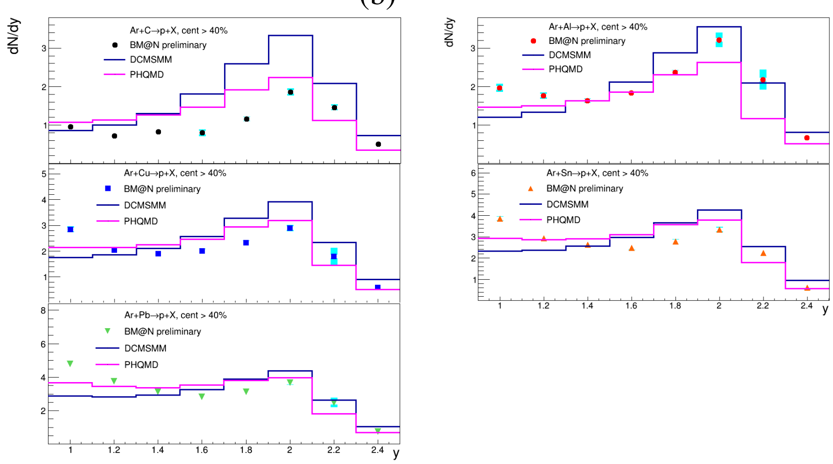

Figure 16: Rapidity spectra dN/dy of protons produced in Ar+C, Al, Cu, Sn, Pb interactions with centrality 0-40% (a) and 40-100% (b). The results are integrated over p_T. The vertical bars and boxes represent the statistical and systematic uncertainties, respectively. The predictions of the DCM-SMM and PHQMD models are shown as blue and magenta lines.

(a)

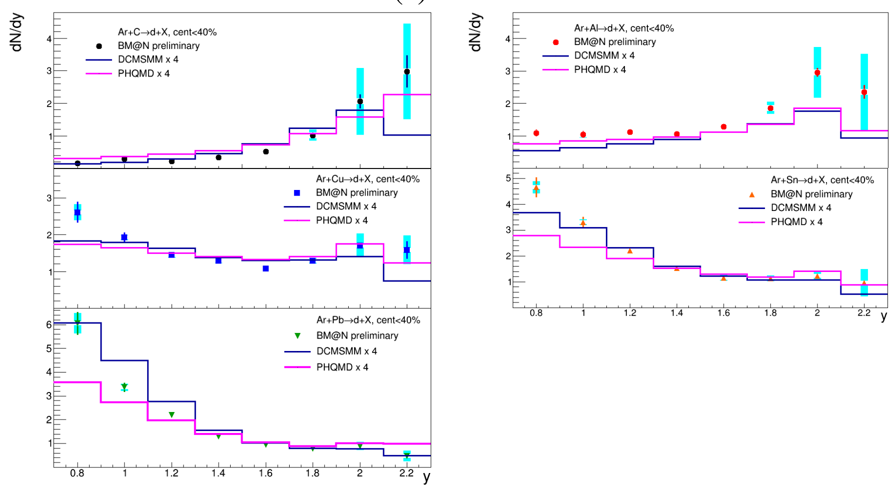

(b)

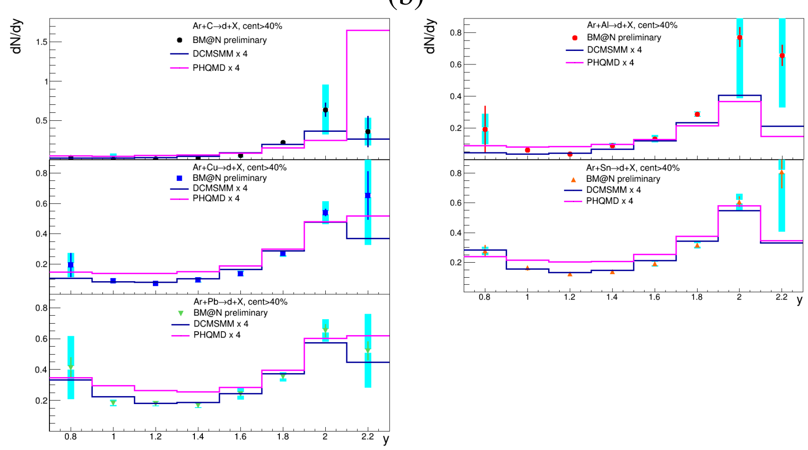

Figure 17: Rapidity spectra dN/dy of deuterons produced in Ar+C,Al, Cu, Sn, Pb interactions with centrality 0-40% (a) and 40-100% (b). The results are integrated over p_T. The vertical bars and boxes represent the statistical and systematic uncertainties, respectively. The predictions of the DCM-SMM and PHQMD models, multiplied by a factor 4, are shown as blue and magenta lines.

(a)

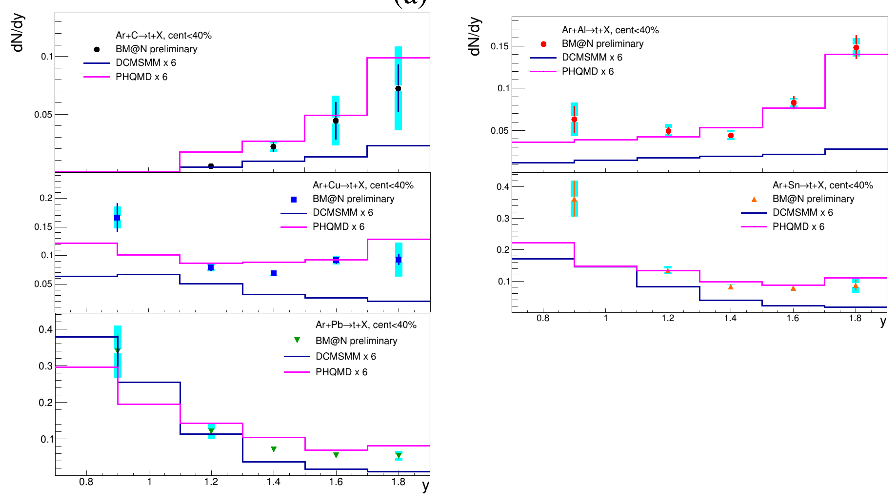

(b)

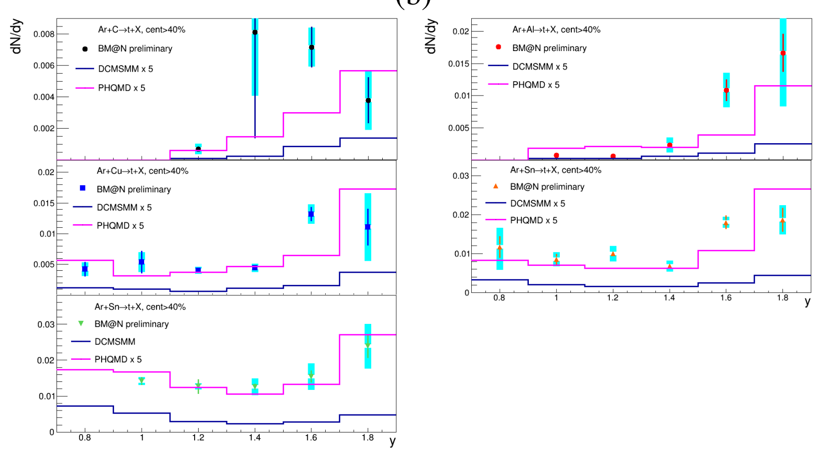

Figure 18: Rapidity spectra dN/dy of tritons produced in Ar+C,Al, Cu, Sn, Pb interactions with centrality 0-40% (a) and 40-100% (b). The results are integrated over p_T. The vertical bars and boxes represent the statistical and systematic uncertainties, respectively. The predictions of the DCM-SMM and PQHMD models, multiplied by factors 6 in (a) and 5 in (b), are shown as blue and magenta lines.

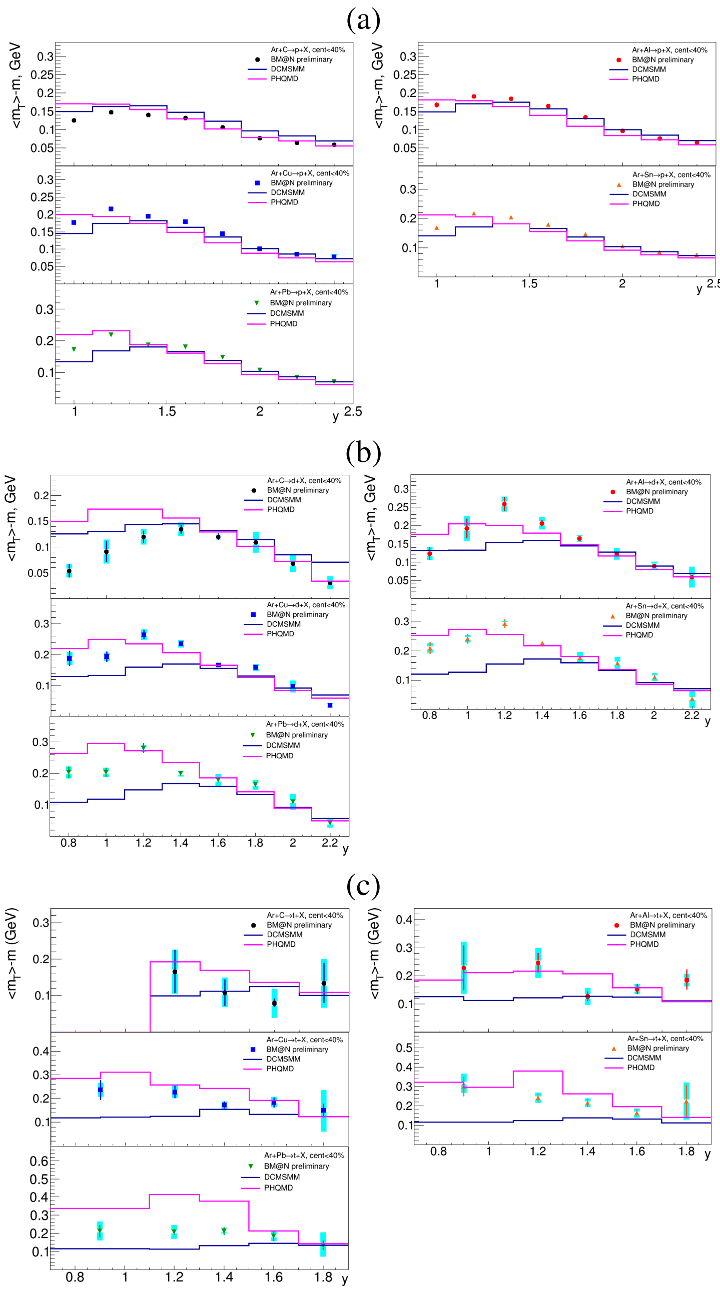

Figure 19: Rapidity y dependence of the mean transverse kinetic energy $\langle m_T \rangle - m$ determined from the fits of the m_T spectra of protons (a), deuterons (b) and tritons (c) in Ar+C, Al, Cu, Sn, Pb interactions with centrality 0-40%. The vertical bars and boxes represent the statistical and systematic uncertainties, respectively. The predictions of the DCM-SMM and PHQMD models are shown as blue and magenta lines.

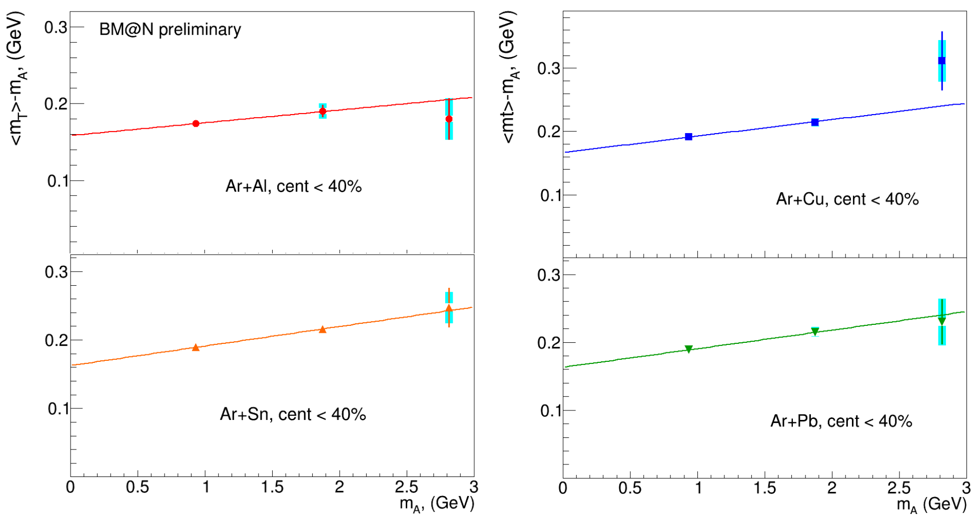

Figure 20: Dependence of the mean transverse kinetic energy $\langle m_T \rangle - m$ on the mass of the nuclear fragment measured in Ar+Al,Cu,Sn,Pb collisions with centrality 0-40%. Linear fits to the data points are indicated by dashed lines.

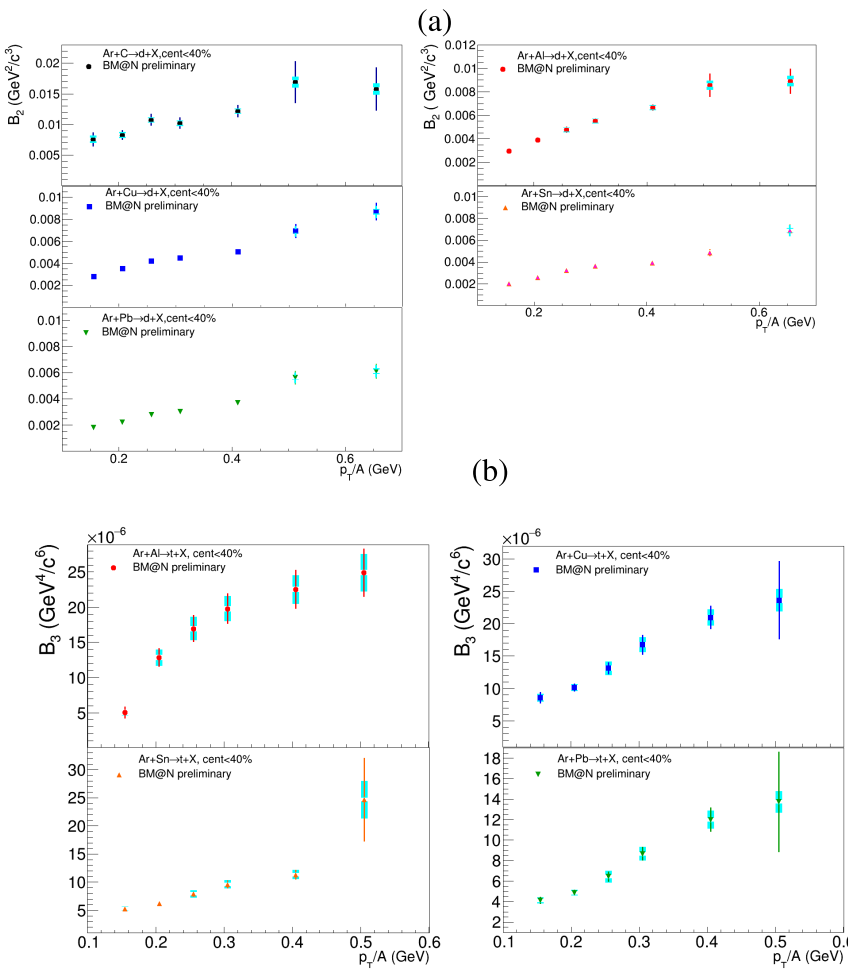

Figure 21: Coalescence parameter B_2 for deuterons (a) and B_3 for tritons (b) measured as a function of p_T/A in Ar+A collisions with centrality 0-40%.

(a)

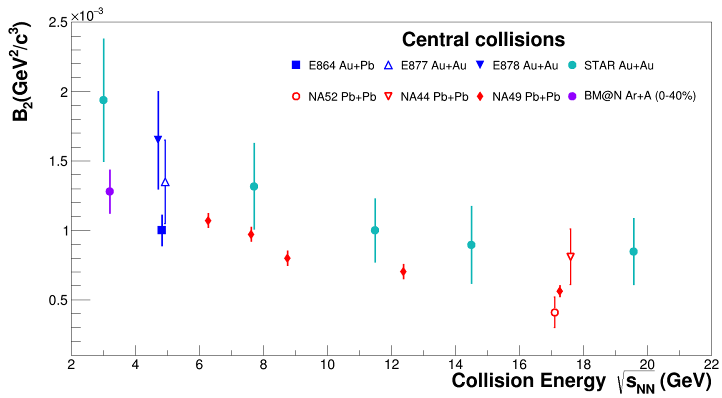

(b)

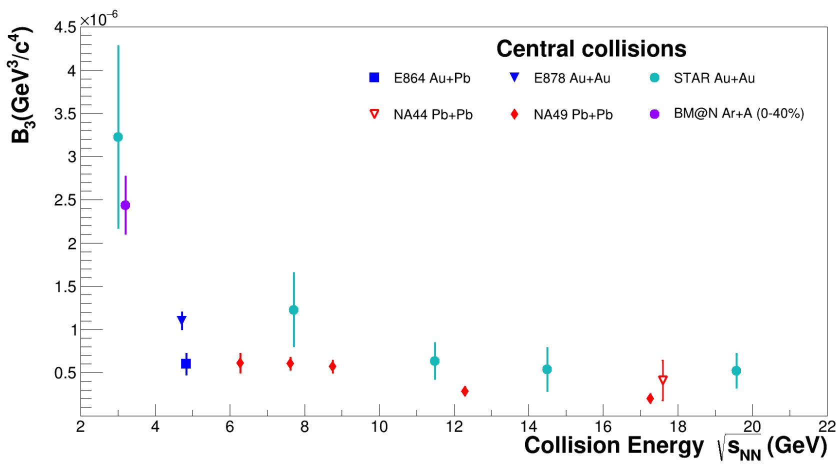

Figure 22: Coalescence parameters $B_2(p_T = 0)$ (a) and $B_3(p_T = 0)$ (b) for deuterons and tritons as a function of the centre-mass energy of nucleus-nucleus interactions. The BM@N result is the weighed average value calculated for Ar+Al,Cu,Sn,Pb interactions with centrality 0-40%.

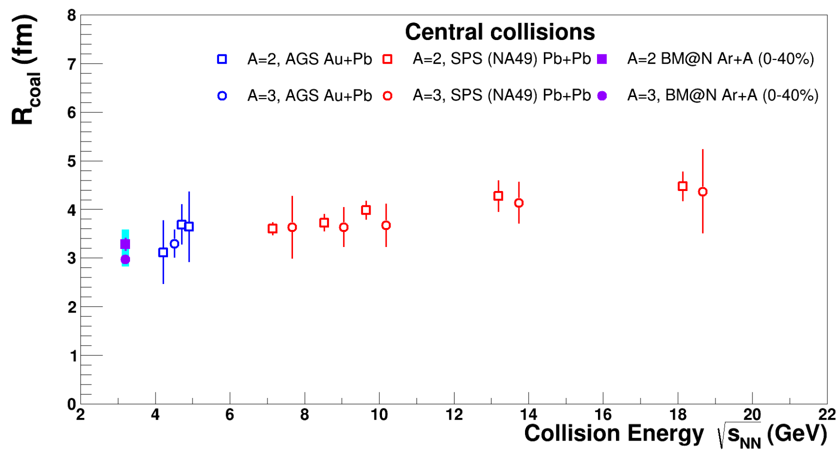

Figure 23: Coalescence radii R_{coal} for deuterons and tritons as a function of the centre-mass energy of nucleus-nucleus interactions. The BM@N result is the weighed average value calculated for Ar+Al,Cu,Sn,Pb interactions with centrality 0-40%.

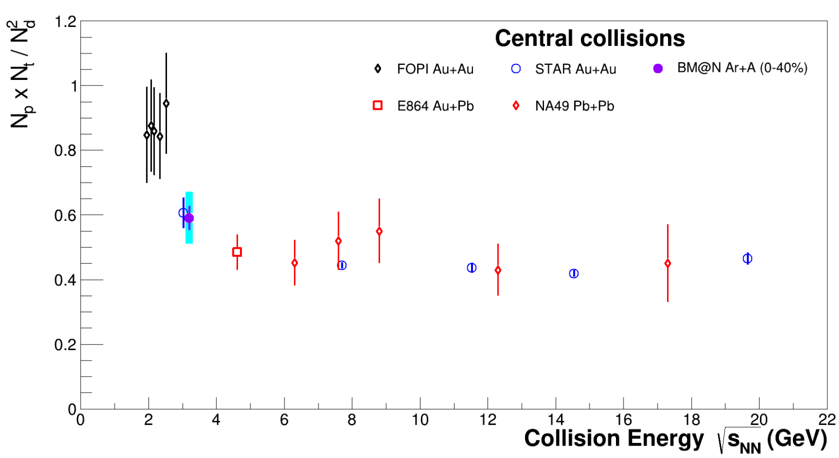

Figure 24: Compound yield ratio $N_p \cdot N_t / N_d^2$ of protons (N_p) and tritons (N_t) to deuterons (N_d^2) as a function of the centre-mass energy of nucleus-nucleus interactions. The BM@N result is the weighed average value calculated for Ar+Al,Cu,Sn,Pb interactions with centrality 0-40%.